Synthesis and optical properties of phenanthrimidazole derivatives for organic electroluminescent devices

Journal:	*New Journal of Chemistry*
Manuscript ID:	NJ-ART-09-2014-001515.R1
Article Type:	Paper
Date Submitted by the Author:	08-Oct-2014
Complete List of Authors:	Jayabharathi, Jayaraman; Annamalai University, Chemistry Ramanathan, Periyasamy; Annamalai university, chemistry Thanikachalam, Venugopal; Annamalai University, Chemistry

Synthesis and optical properties of phenanthrimidazole derivatives for organic electroluminescent devices

Jayaraman Jayabharathi*, Periyasamy Ramanathan, Venugopal Thanikachalam

Department of Chemistry, Annamalai University, Annamalainagar 608 002, Tamilnadu, India.

* Address for correspondence
Dr. J. Jayabharathi
Professor of Chemistry
Department of Chemistry
Annamalai University
Annamalainagar 608 002
Tamilnadu, India.
Tel: +91 9443940735
E-mail: jtchalam2005@yahoo.co.in

Synthesis and optical properties of phenanthrimidazole derivatives for organic electroluminescent devices

Jayaraman Jayabharathi*, Periyasamy Ramanathan, Venugopal Thanikachalam

Department of Chemistry, Annamalai University, Annamalainagar 608 002, Tamilnadu, India.

Abstract

Five phenanthrimidazole derivatives namely, 2-(naphthalen-1-yl)-1H-phenanthro [9,10-d]imidazole (**1**); 2-(naphthalen-1-yl)-1-phenyl-1H-phenanthro[9,10-d]imidazole (**2**); 2-(naphthalen-1-yl)-1-p-tolyl-1H-phenanthro[9,10-d]imidazole (**3**); 1-(4-methoxyphenyl)-2-(naphthalen-1-yl)-1H-phenanthro[9,10-d]imidazole (**4**) and 1-(3,5-dimethylphenyl)-2-(naphthalen-1-yl)-1H-phenanthro[9,10-d]imidazole) (**5**) were synthesised using TiO_2 (R) nanosemiconductor as catalyst under solvent free condition and characterised by NMR and single crystal XRD techniques. Their photophysical, electrochemical and electroluminescent properties were carefully analysed. Highly efficient Alq_3-based organic light emitting devices have been developed using phenanthrimidazoles as a functional layer between NPB [4,4-bis(N-(1-naphthyl)-N-phenylamino)biphenyl] and Alq_3 [tris(8-hydroxyquinoline)aluminium] layers. From the device of ITO/NPB/**4**/Alq_3/LiF/Al, a maximum luminous efficiency of 5.99 cd A^{-1} was obtained with a maximum brightness of 40623 cd m^{-2} and power efficiency of 5.25lm/w^{-1}.

Keywords: TiO_2 (R), Phenanthrimidazole; OLED device; Single crystal XRD; TG-DTA.

1. Introduction

Arylimidazoles play important role in materials science and medicinal chemistry due to their optoelectronic properties and high thermal stabilities [1-7]. Substituted imidazoles are extensively used as glucagon receptors [8], cannabinoid receptor antagonists [9] and modulators of glycoprotein mediated multidrug resistance [10], antibacterial [11], anti-allergic [12], analgesic [13], antitumor [14] and pesticides [15]. Many of the reported synthetic protocols for imidazoles [16-27] suffer from disadvantages such as use of toxic and chlorinated organic solvents, acidic conditions, complex work-up and purification, side reactions, low yield and use of hazardous and expensive reagents. Thus the development of a new catalyst is essential to overcome these shortcomings and to fulfill the criteria of a milder reaction conditions, higher yield and reusability of catalyst.

Titanium dioxide find widespread industrial applications [28-32] and its utility has been extended to the photodegradation of pesticides [33] and carcinogenic dyes [34, 35]. From a synthetic point of view, titanium dioxide has been used as a green, inexpensive, mild and recyclable heterogeneous Lewis acid potential catalyst in certain organic transformations like Beckmann rearrangement [36], Fridel-Crafts acylation [37], Biginelli condensation [38] and also in the synthesis of dihydropyrazines [39], piperazines [40], quinoxalines [41] and photocatalytic oxidation of amines [42].

Highly efficient electroluminescence (EL) have been obtained from a bilayer device composed of NPB and Alq_3 which are the most widely used hole-transporting and electron-transporting as well as host emitting materials, respectively in organic light-emitting diodes (OLEDs) due to their high thermal stability [43-45]. However, the electron and hole mobilities in Alq_3 and NPB are at the level of 10^{-4}–10^{-5} and 10^{-3}–10^{-4} cm^2 V^{-1} s^{-1}, respectively, in an electric field of 2 x 10^6 V cm^{-1} [46,47] which gives rise to an accumulation of excess holes at the NPB/Alq_3 boundary. Insertion of an anodic buffer layer including organic [48] and

inorganic [49] materials between indium-tin oxide (ITO) and hole-transporting layer (HTL) as a hole injection layer (HIL) could control the hole injection and resulted in enhanced luminous efficiency (LE) [50]. In this article, we report a simple and straightforward one-pot synthesis of naphthyl phenanthrimidazoles [51] in good yield using sol-gel synthesised nano titanium dioxide as an inexpensive heterogeneous and recyclable non-toxic catalyst under solvent free solid-phase condition. We also present the significant enhancement of the EL performance by inserting the newly synthesised naphthyl phenanthrimidazoles [52] as a functional layer with the thickness of tens of nanometers between NPB and Alq_3 layer in the device structure, ITO/NPB/naphthyl phenanthrimidazoles/Alq_3/LiF/Al.

2. Experimental

2.1. Chemicals

1-naphthaldehyde and phenanthrene-9,10-dione were supplied by Sigma-aldrich (St.Louis, USA). Aniline, 4-methylaniline, 4-methoxyaniline and 3,5-dimethylaniline were used of analytical grade and received from S.D.Fine (Mumbai, India). The solvents used were of spectroscopic grade supplied by Himedia (Chennai, India).

2.2. Synthesis of nanocrystalline TiO_2 by sol- gel method

The TiO_2 nanocrystal were prepared by sol- gel hydrolysis of titanium(IV) isopropoxide, followed by calcination. About 1ml of titanium isopropoxide (Merck, 97%) was dissolved in 20 ml isopropyl alcohol (Merck, 95%) and the solution was dropped slowly into 10 ml of distilled water and the pH was adjusted to 2. After stirring water was added to alkoxide solution, the formed white sol-gel of hydrous oxide was stirred vigorously for 4 hours at room temperature and then allowed to age overnight. The solid was centrifuged and was redispersed in ethanol to minimise agglomeration. This process was repeated for five times and the solid was filtered. The resulting material was then dried and calcinated upto 800 °C for 2 hr. The sample was characterised by x-ray diffraction (XRD), scanning electron micrograph (SEM),

diffused reflectance spectra (DRS) and solid state photoluminescence spectroscopy. From these results it is found that high acidity [pH 2] favor for the formation of rutile phase TiO_2 [53, 54].

2.3. Synthesis of polysubstituted imidazoles

A mixture of naphthaldehyde (1 mmol), phenanthrene-9,10-dione (1 mmol), arylamine (1 mmol) and ammonium acetate (1mmol) with TiO_2 (1 mol%) as catalyst was stirred at 120 °C with continuous stirring with a bar magnet. The progress of the reaction was monitored by TLC (Scheme 1). After completion of the reaction, 10 ml ethyl acetate was added to the reaction mixture and shaken well to dissolve the organic components and the mass filtered to separate out TiO_2 and the residue was washed with ethyl acetate. The solid TiO_2 residue was further washed with hot acetone and then dried up. The product was purified by column chromatography using benzene: ethyl acetate (9:1) as the eluent. The newly synthesised phenanthrimidazoles have been characterised by ^1H and ^{13}C NMR and mass (MS) spectra.

2.3.1. 2-(Naphthalen-1-yl)-1H-phenanthro[9,10-d]imidazole (**1**)

M.p. 262 ºC., Anal. calcd. for $C_{25}H_{16}N_2$: C, 87.18; H, 4.68; N, 8.13. Found: C, 86.98; H, 4.52; N, 7.95. ^1H NMR (400 MHz, DMSO): δ 10.41 (s, 1H), 7.37 (s, 4H), 8.77 (d, J = 7.2 Hz, 3H), 7.90 (d, J = 8.0 Hz, 2H), 7.82 (d, J = 7.2 Hz,1H), 7.66 (t, 4H), 7.54-7.45 (m, 3H). ^{13}C NMR (400 MHz, $CDCl_3$): δ 121.83, 123.78, 124.97, 125.47, 125.89, 126.38, 127.12, 127.29, 127.58, 127.88, 128.37, 128.47, 130.16, 131.30, 133.92, 148.87. MS: m/z. 344 [M+].

2.3.2. 2-(Naphthalen-1-yl)-1-phenyl-1H-phenanthro[9,10-d]imidazole (**2**)

M.p. 265 ºC., Anal. calcd. for $C_{31}H_{20}N_2$: C, 88.54; H, 4.79; N, 6.66. Found: C, 88.36; H, 4.68; N, 6.48. ^1H NMR (400 MHz, DMSO): δ 8.89 (d, J = 7.6 Hz, 1H), 8.80 (d, J = 8.4 Hz, 1H), 8.75 (d, J = 7.6 Hz, 1H), 7.99 (d, J = 5.6 Hz, 1H),7.83 (d, J = 7.6 Hz, 2H), 7.74 (t, 1H), 7.67 (t, 1H), 7.53 (t, 1H), 7.48-7.43 (m, 3H), 7.35-7.29 (m, 6H). ^{13}C NMR (400 MHz, $CDCl_3$): δ 121.07, 122.89, 123.01, 123.18, 124.16, 124.48, 125.02, 125.65, 126.02, 126.17, 126.34,

126.88, 127.38, 127.44, 128.05, 128.15, 128.34, 128.49, 129.28, 129.48, 129.55, 129.73, 133.21, 133.47, 137.38, 138.04, 150.48. MS: m/z. 420 [M+].

2.3.3. 2-(Naphthalen-1-yl)-1-p-tolyl-1H-phenanthro[9,10-d]imidazole (**3**)

M.p. 248 ºC., Anal. calcd. for $C_{32}H_{22}N_2$: C, 88.45; H, 5.10; N, 6.45. Found: C, 88.28; H, 4.97; N, 6.31. ^{1}H NMR (400 MHz, DMSO): δ 2.32 (s, 3H), 8.88 (d, J = 7.6 Hz, 1H), 8.79 (d, J = 8.4 Hz, 1H), 8.73 (d, J = 8.0 Hz, 1H), 7.96 (d, J = 7.2 Hz, 1H), 7.80 (d, J = 8.0 Hz, 2H), 7.20 (d, J = 7.6 Hz, 2H), 7.10 (d, J = 8.0 Hz, 2H), 7.71 (t, 1H), 7.65 (t, 1H), 7.53 (t, 1H), 7.43 (q, 3H) 7.35-7.24 (m, 4H). ^{13}C NMR (400 MHz, DMSO): δ 21.31, 121.11, 122.87, 123.12, 123.20, 124.14, 124.50, 124.70, 125.00, 125.10, 125.62, 126.04, 126.14, 126.35, 126.83, 127.38, 127.53, 127.77, 128.15, 128.34, 128.39, 129.28, 129.47, 129.67, 130.20, 133.23, 133.44, 133.76, 135.32, 137.27, 139.29, 150.63. MS: m/z. 434 [M+].

2.3.4. 1-(4-Methoxyphenyl)-2-(naphthalen-1-yl)-1H-phenanthro[9,10-d]imidazole (**4**)

M.p. 272 ºC., Anal. calcd. for $C_{32}H_{22}N_2O$: C, 85.31; H, 4.92; N, 6.22. Found: C, 85.15; H, 4.78; N, 6.08. ^{1}H NMR (400 MHz, DMSO): δ 3.72 (s, 3H), 8.96 (d, J = 8.4 Hz, 1H), 8.9 (d, J = 8.4 Hz, 1H), 8.66 (d, J = 7.6 Hz, 1H), 7.89 (d, J = 8.0 Hz, 1H), 7.76 (d, J = 7.2 Hz, 1H), 7.57 (d, J = 7.6 Hz, 1H), 7.38 (t, 1H), 7.20 (d, J = 8.0 Hz, 1H), 6.94 (d, J = 8.4 Hz, 2H), 7.96 (t, 2H), 7.69(t, 2H), 7.55-7.42 (m, 5H). ^{13}C NMR (400 MHz, DMSO): δ 55.28, 114.62, 120.27, 121.98, 122.59, 123.66, 124.42, 124.67, 125.19, 125.60, 125.78, 126.20, 126.69, 126.82, 126.86, 127.24, 127.42, 127.64, 128.04, 128.09, 128.29, 128.41, 129.50, 129.52, 129.72, 129.95, 132.35, 132.76, 136.28, 150.47, 159.47. m/z. 450 [M+].

2.3.5. 1-(3,5-Dimethylphenyl)-2-(naphthalen-1-yl)-1H-phenanthro[9,10-d]imidazole (**5**)

M.p. 261 ºC., Anal. calcd. for $C_{33}H_{24}N_2$: C, 88.36; H, 5.39; N, 6.25. Found: C, 88.19; H, 5.26; N, 6.09. ^{1}H NMR (400 MHz, DMSO): δ 2.17 (s, 6H), 8.96 (d, J = 8.0 Hz, 1H), 8.91 (d, J = 8.0 Hz, 1H), 8.64 (d, J = 7.6 Hz, 1H), 7.97 (t, 2H), 7.91 (d, J = 7.2 Hz, 1H), 7.76 (d, J = 7.2 Hz, 1H), 7.74 (d, J = 6.4 Hz, 2H), 7.08 (s, 1H), 7.16 (t, 2H), 7.36-7.40 (m, 3H),7.60-

7.48 (m, 3H). ^{13}C NMR (400 MHz, DMSO): δ 20.54, 120.36, 121.99, 122.45, 123.66, 124.42, 124.66, 125.22, 125.44, 125.66, 125.83, 126.06, 126.22, 126.33, 126.71, 126.76, 127.00, 127.23, 127.45, 127.62, 127.90, 128.04, 128.29, 128.40, 129.54, 131.01, 132.28, 132.75, 136.27, 137.28, 138.90, 150.06. MS: m/z. 448 [M+].

2.4. Measurements

XRD patterns were recorded for the centrifuged and dried samples using X–ray Rigaku diffractometer with Cu K_α source (30 kV, 100 mA), at a scan speed of 3.0000 deg/min, step width of 0.1000 deg, in a 2θ range of 20-80°. The energy dispersive X-ray (EDS) spectra of the nanosemiconductors were recorded with a JEOL JSM-5610 scanning electron microscope (SEM) equipped with back electron (BE) detector and EDX. The sample was placed on an adhesive carbon slice supported on copper stubs and coated with 10 nm thick gold using JEOL JFC- 1600 auto fine coater prior to measurement. The ^{1}H and ^{13}C NMR spectra at 400 and 100 MHz, respectively were obtained at room temperature using a Bruker 400 MHz NMR spectrometer (Bruker biospin, California, USA). The mass spectra were obtained using a Thermo Fischer LC-Mass spectrometer in fast atom bombardment (FAB) mode (Thermo, France). The UV-vis and photoluminescence spectra were recorded with Perkin Elmer Lambda 35 UV-vis spectrophotometer and PerkinElmer LS55 fluorescence spectrometer, respectively.

The lifetime measurements were carried out with a nanosecond time correlated single photon counting (TCSPC) spectrometer Horiba Fluorocube-01-NL lifetime system with Nano LED (pulsed diode excitation source) as the excitation source and TBX-PS as detector. The quantum yields were measured by comparing the emission intensities of a standard sample and the unknown sample [55-57] using the formula, $\Phi_{unk} = \Phi_{std}\left(\frac{I_{unk}}{I_{std}}\right)\left(\frac{A_{std}}{A_{unk}}\right)\left(\frac{\eta_{unk}}{\eta_{std}}\right)^2$, Φ_{unk} and Φ_{std} are the quantum yield of the sample and the standard, respectively; I_{unk} and I_{std} are the integrated emission intensities of the sample and the standard, respectively. A_{unk} and A_{std} are the

absorbance of the sample and the standard at the excitation wavelength, respectively. η_{unk} and η_{std} are the refractive index of the sample and standard solutions, respectively. The cyclic voltammetry analyses were performed with CHI electrochemical analyser 604C (CHI electrochemical analyser, USA) at a scan rate of 100 mV s^{-1} using 0.1 M tetra-(*n*-butyl)-ammonium hexafluorophosphate as supporting electrolyte with Ag/Ag^+ (0.01 M $AgNO_3$) as the reference electrode and Pt electrode as the working electrode, standardised for the redox couple ferricinium/ferrocene. All solutions were purged with a nitrogen stream for 10 min before measurement. Thermal analysis of the phenanthrimidazoles was made with NETZSCH-Geratebau Gmbh thermal analysis STA 409 PCO. The differential scanning calorimetric (DSC) and thermogravimetric analyses (TGA) were made under nitrogen atmosphere (100 mL min^{-1}). The sensitivity of the instrument was set at 0.01 μg and the sample (10 mg) was heated from 30 to 700° C at the rate of 10 or 15 or 20 K min^{-1}. DFT calculations were performed with Gaussian-03 [58] package.

2.5. Device fabrication

The EL devices based on the phenanthrimidazoles were fabricated by vacuum deposition of the materials at 5 x 10^{-6} torr onto a clean glass precoated with a layer of indium tin oxide as the substrate with sheet resistance of 20 Ω/square. The glass was cleaned by sonication successively in a detergent solution, acetone, methanol and deionised water before use. Organic layers were deposited onto the substrate at a rate of 0.1nm s^{-1}. LiF and Alq_3 were thermally evaporated onto the surface of organic layer. The thickness of the organic materials and the cathode layers were controlled using a quartz crystal thickness monitor. A series of devices (I, II, III, IV and V) with multilayer configuration of ITO/NPB (60 nm)/**1-5** (20 nm)/Alq_3 (30 nm)/LiF (1 nm)/Al (100 nm) were fabricated. Measurement of current, voltage and light intensity were made simultaneously using a Keithley 2400 sourcemeter (Keithley,

Cleveland, Ohio). The EL spectra of the devices were carried out in ambient atmosphere without further encapsulations.

3. Results and discussion

3.1. Characterisation of nano TiO_2 (R)

Nanocrystalline rutile phase of TiO_2 was obtained by sol–gel method, characterised by X-ray diffraction, high resolution scanning electron microscopy and energy dispersive, UV–visible diffuse reflectance and solid state photoluminescence spectroscopies. Figure 1 displays the X-ray diffraction pattern (XRD) of rutile phase of TiO_2 nanoparticles and the diffraction pattern of TiO_2(R) matches with the JCPDS pattern of tetragonal primitive (89-4920). The crystal constants a and c are 4. Å and 2.953 Å, respectively. The average crystallite size (L) deduced from the XRD result is 20.44 nm. The Scherrer equation, $L = 0.9\lambda/\beta\cos\theta$ (where λ is the wavelength of the X-ray used, θ is the diffraction angle and β is the full width at half maximum of the peak) was used to obtain the mean crystalline size. The specific surface area (S) of the nanocrystal has been deduced by employing the relationship, $S = 6/\rho L$ (ρ is the material density). The calculated surface area for rutile phase of TiO_2 is 51.72 m^2/g.

The scanning electron micrograph (SEM) of TiO_2 (R) nanoparticle is displayed in Figure 1. The DRS of rutile TiO_2 is displayed in Figure 2 which is presented in terms of $F(R)$, deduced from the recorded reflectance (R) by application of the Kubelka-Munk algorithm [$F(R) = (1 - R)^2/2R$]. The absorption edge of rutileTiO_2 is 389 nm and the deduced absorption edge provides the band gap of rutile TiO_2, as 3.19 eV. The band gap of the synthesised rutile TiO_2 is larger than the literature value. This is because of the smaller size of the synthesised nanoparticles. Quantum confinement effect increases the band gap energy.

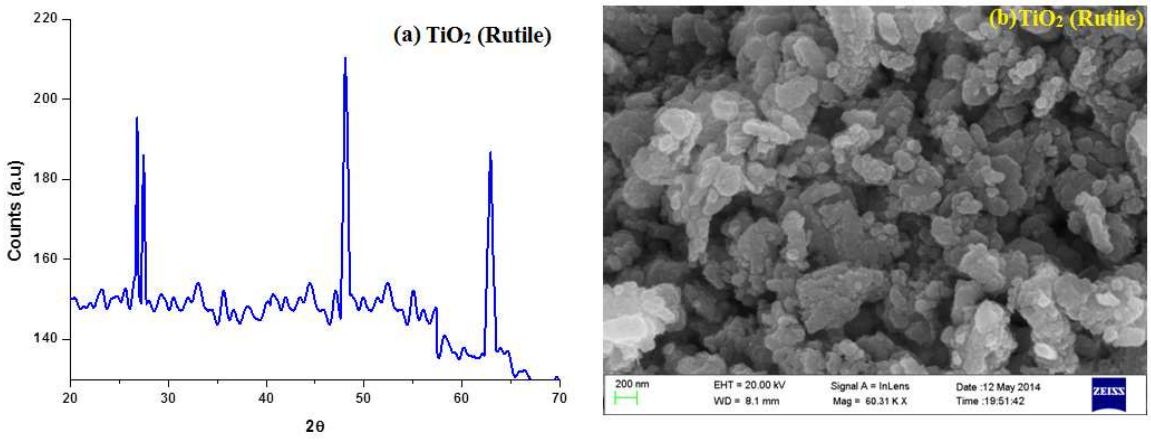

Figure 1. (**a**) X-ray diffraction pattern (XRD) of TiO_2 (Rutile); (**b**) SEM image of TiO_2 (Rutile)

Figure 2 displays the solid state photoluminescence spectra of the synthesised rutile TiO_2 nanocrystals. Nanocrystals were excited at 340 nm and the solid emission spectrum of rutile TiO_2 mainly consist of four emission bands: a strong violet emission at 411 nm (3.01 eV), a blue band at 450 nm (2.75 eV), a blue-green band at 482 nm (2.57 eV) and a weak green band at 530 nm (2.34 eV). The two peaks at 482 and 530 nm are attributed to the transition from the oxygen vacancies with two trapped electrons and one trapped electron to the valence band of TiO_2, respectively. The energy levels related to the two kinds of the oxygen vacancies are located at 0.51 and 0.82 eV below the conduction band (CB) of TiO_2, respectively. Because of the existence of the energy levels of oxygen vacancies, first the photogenerated electrons in the CB is likely to reach the oxygen vacancies through a non-radiative process and then recombine with the photogenerated holes in the valence band (VB) accompanied by the emission of fluorescence. The broad band in the visible region is also ascribed to the radiative recombination of exciton of the shallow traps identified with oxygen vacancies and Ti^{4+} adjacent to oxygen vacancies [59].

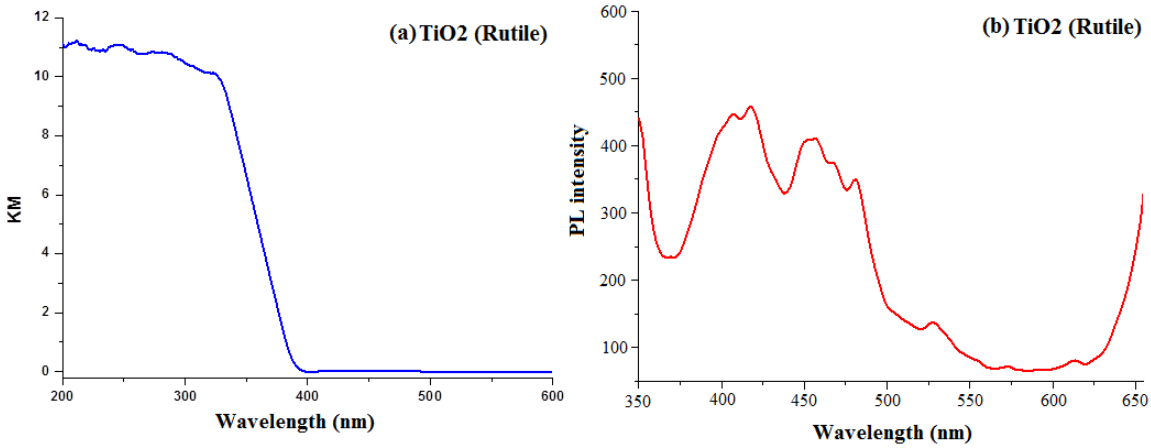

Figure 2. (**a**) Diffused reflectance spectra of TiO_2 (Rutile); (**b**) Solid state photoluminescence spectra of TiO_2 (Rutile)

3.2. Catalytic activity of TiO_2 (R) semiconductor

Initially, we have carried out the condensation reaction in the presence of TiO_2(R) (1mol %), 1-naphthaldehyde (1 mmol), ammonium acetate (1 mmol) and arylamine (1 mmol) in different solvents such as water, ethanol, methanol, chloroform and acetonitrile under refluxing and also in solvent-free condition at 120 °C (Scheme 1). From these experiments, it was clearly demonstrated that the solvent-free condition is the best for phenanthrimidazole synthesis. In the absence of catalyst under solvent-free condition at room temperature the yield is very poor even after 24 hr. To enhance the yield of the desired product, the temperature of the reaction was increased to 180 ºC, but no appreciable increment in the product yield was observed. We found that presence of a catalytic amount of TiO_2(R) under solvent-free condition is the best for this synthesis; maximum yield (82%) was obtained at 30 min on loading with 1mol% of TiO_2 (R) at 120 °C (Table 1). Moreover, TiO_2 can be recovered and reused several times without significant loss of activity. High product yield, shorter reaction time, low catalyst loading and easy work-up procedure, make this procedure quite simple and more convenient. Our methodology could be a valid contribution to the existing processes of imidazole synthesis.

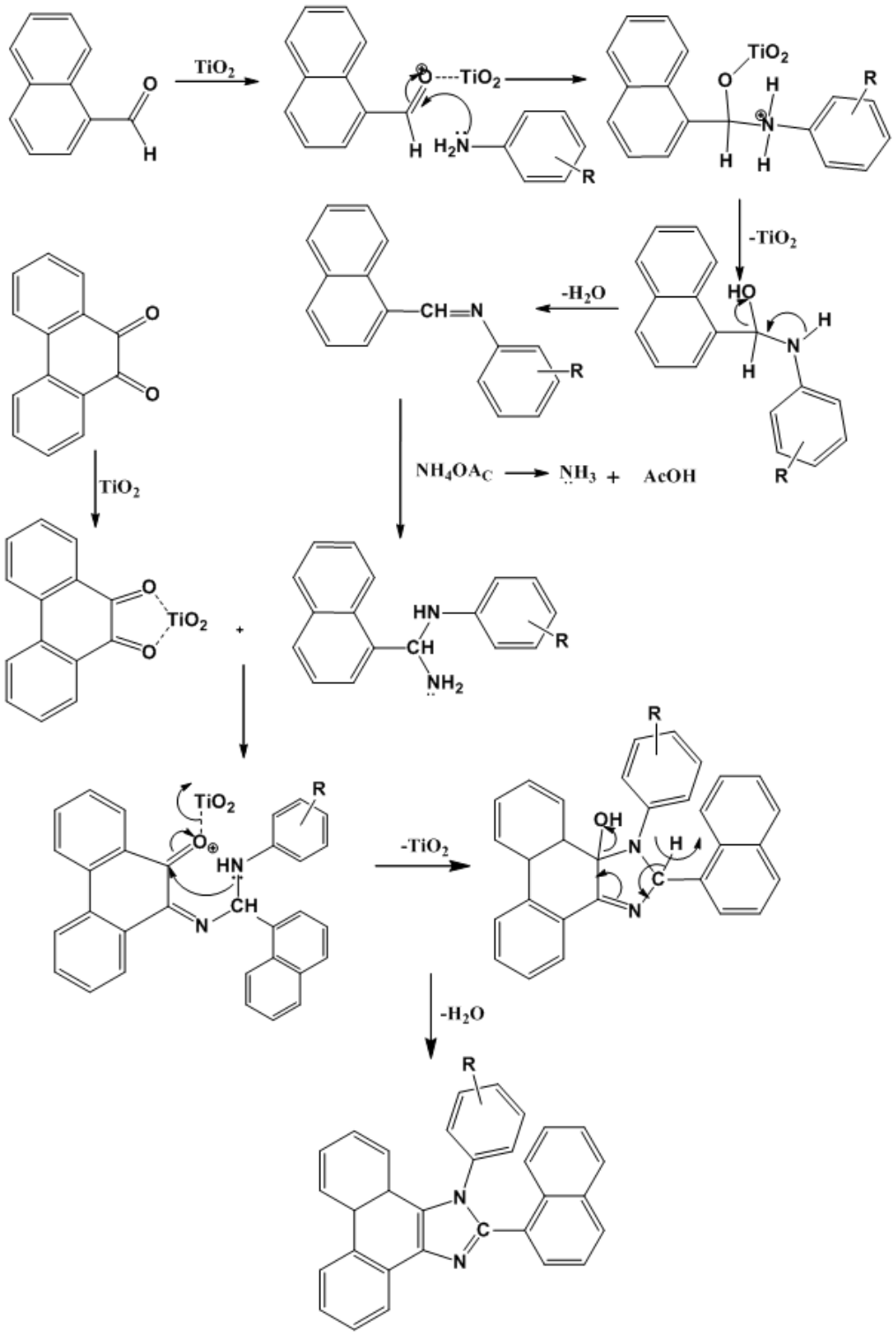

Scheme 1. Possible mechanism for catalytic synthesis of phenanthrimidazoles

Table 1. Effect of TiO_2 (R) catalyst and temperature in the synthesis of phenanthrimidazoles

Entry	Temp (°C)	solvent	TiO_2 (R)		TiO_2 (R) (mol %)
			Time (min)	Yield (%)	
1	r.t	Solvent-free	130 (380)	70(Trace)	0.1
2	50	Solvent-free	65(250)	72(22)	0.1
3	70	Solvent-free	30(70)	76(45)	0.1
4	90	Solvent-free	25(90)	80(53)	0.1
5	120	Solvent-free	30	82	1
6	120	Solvent-free	25	85	2
7	120	Solvent-free	45	88	10
8	120	Water	100	35	1
9	120	Ethanol	40	65	1
10	120	Methanol	50	70	1
11	120	Chloroform	140	42	1
12	120	Acetonitrile	95	62	1

values in the parenthesis corresponds to without catalyst

3.3. XRD characterisation of 1-(4-methoxyphenyl)-2-(naphthalen-1-yl)-1H-phenanthro [9,10-d] imidazole (**4**)

The naphthyl phenanthrimidazoles have been synthesised using modified Debus-Radziszewski method, with the use of TiO_2(R) as catalyst [60]. 1-(4-methoxyphenyl)-2-(naphthalen-1-yl)-1H-phenanthro[9,10-d]imidazole is a monoclinic crystal and crystallizes in P21/c space group with cell dimensions of a = 12.3316 (7) A, b = 21.3475 (11) A and c = 8.8212 (5) A and the ORTEP diagram is presented in Figure 3. The imidazole unit forms dihedral angles of -86.9º (17) [N(2)-C(15)-C(16)-C(17)] and -102.3º(17) [C(14)-N(2)-C(26)-C(31)] with the adjacent naphthyl and methoxyphenyl ring. In the crystal, molecules are consolidated into a three-dimensional architecture by π–π stacking interactions. The electron donating naphthyl ring and the electron accepting phenanthrimidazole moiety would lead to intermolecular electrostatic interaction [61]. Optimization of 1-(4-methoxyphenyl)-2-(naphthalen-1-yl)-1H-phenanthro [9,10-d]imidazole has been performed by DFT at B3LYP/6-31G(d,p) level using Gaussian-03. The optimized parameters namely, bond lengths, bond angles and dihedral angles are slightly higher than that of XRD values (Table 2). Because the theoretical calculations are of isolated molecule in the gaseous phase and the XRD results are of the molecule in the solid state. Thermal properties have been investigated by differential scanning calorimetry (DSC) and thermal gravimetric analyses (TGA) under nitrogen atmosphere and the results are displayed in Figure 3. All phenanthrimidazoles exhibit good thermal stability and the decomposition temperature with 5% weight loss (T_{d5}) has been measured as 310, 315, 319, 325 and 334 °C for compounds **1-5**, respectively (Table 3). The melting point of phenanthrimidazoles **1-5** measured by DSC is 262, 265, 248, 272 and 261 °C, respectively. On the second heating, no melting points were observed, even though it was given enough time to cool in air. Once it became an amorphous solid, it did not revert to the crystalline state at all. After the sample had cooled to room temperature, a second DSC scan

performed at 10 ^{o}C/min revealed a glass transition temperature (T_g) in the range of 65 to 82 °C. The methoxy phenanthrimidazole **4** has the highest melting point which may due to the intermolecular C–H···π interactions that can induce more condensed molecular packing. The high T_m and T_{d5} values indicate that they could form morphologically stable amorphous film upon vacuum thermal evaporation which is highly important for device fabrication [62] since the high T_m and T_{d5} could improve the life time of the devices.

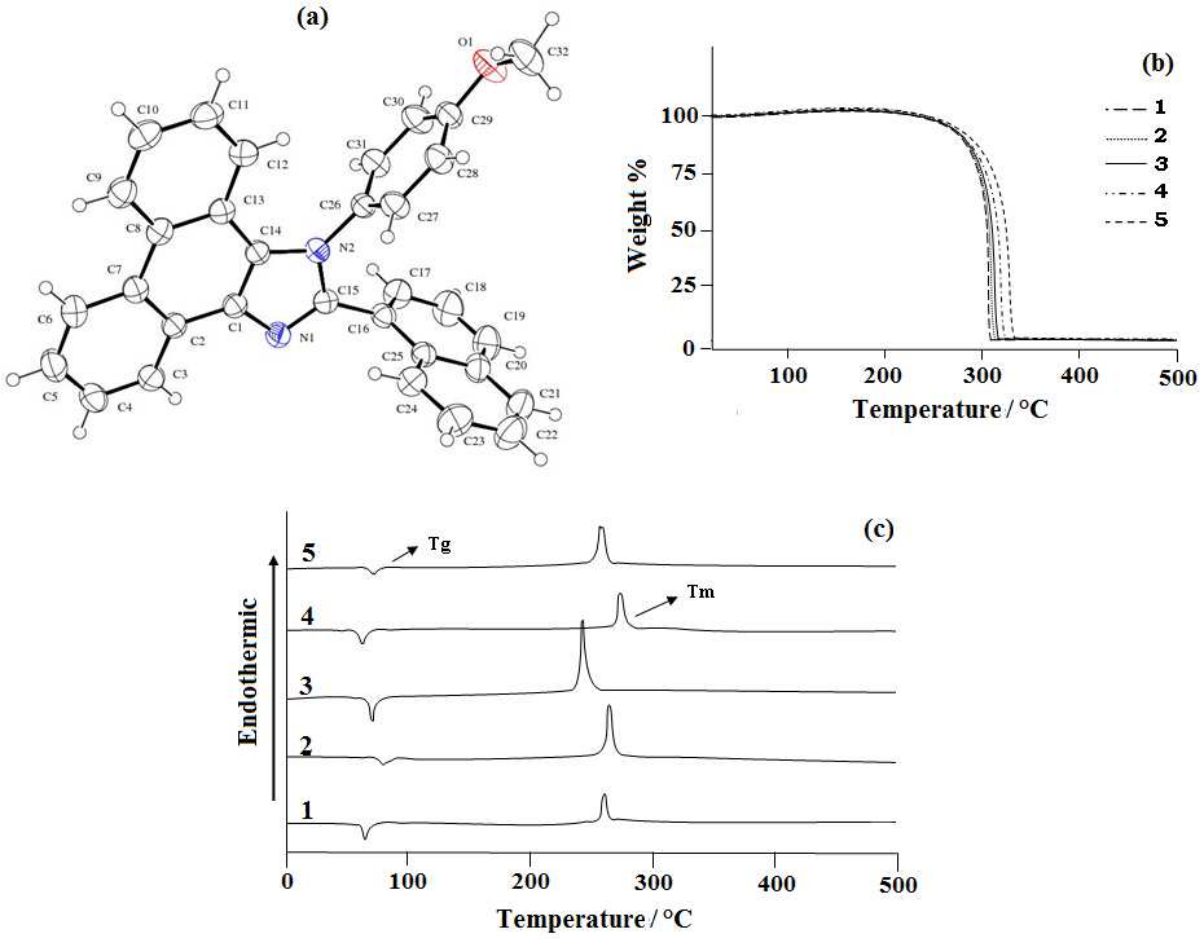

Figure 3. (**a**) ORTEP diagram of 1-(4-methoxyphenyl)-2-(naphthalen-1-yl)-1H-phenanthro[9,10-d]imidazole (**4**); (**b**) TG -DTA (upper); (**c**) DSC (bottom) curves of phenanthrimidazoles at a heating rate of 20 °C min^{-1}

Table 2. Selected bond lengths (Å), bond angles (º) and torsional angles (º) of 1-(4-methoxyphenyl)-2-(naphthalen-1-yl)-1H-phenanthro[9,10-d]imidazole (**4**)

Connectivity	Bond lengths XRD	Connectivity	Bond angles XRD	Connectivity	Torsional angles XRD
C(1)-C(14)	1.3744(1.3746)	C(14)-C(1)-C(2)	121.82(121.84)	N(1)-C(1)-C(14)-N(2)	0.24(0.26)
C(1)-C(2)	1.4279(1.429)	N(1)-C(1)-C(2)	126.92(126.94)	N(1)-C(1)-C(2)-C(3)	-3.2(-3.4)
C(13)-C(14)	1.4349(1.4351)	C(1)-C(14)-C(13)	123.28(123.29)	C(1)-C(2)-C(7)-C(8)	1.71(1.73)
C(1)-N(1)	1.3809(1.3810)	C(14)-C(1)-N(1)	111.22(111.24)	N(1)-C(1)-C(14)-N(2)	0.24(0.26)
C(15)-N(1)	1.3132(1.3135)	N(2)-C(14)-C(13)	131.68(131.69)	N(1)-C(15)-N(2)-C(14)	1.15(1.17)
C(15)-N(2)	1.3710(1.3712)	C(14)-N(2)-C(26)	128.04(128.06)	N(2)-C(15)-C(16)-C(17)	-86.86(-86.88)
C(14)-N(2)	1.3897(1.3899)	C(31)-C(26)-N(2)	120.32(120.34)	N(2)-C(15)-C(16)-C(25)	94.40(94.42)
C(15)-C(16)	1.4779(1.4780)	C(27)-C(26)-N(2)	119.36(119.38)	N(2)-C(26)-C(27)-C(28)	-176.51(-176.53)
C(16)-C(17)	1.363(1.3650)	C(27)-C(26)-C(31)	120.31(120.33)	C(13)-C(14)-N(2)-C(26)	1.6(1.8)
C(16)-C(25)	1.4214(1.423)	C(26)-C(27)-C(28)	120.55(120.57)	C(31)-C(26)-N(2)-C(14)	-102.27(17)
C(17)-C(18)	1.395(1.3970)	C(29)-C(28)-C(27)	119.24(119.25)	C(27)-C(26)-N(2)-C(14)	76.45(76.47)
C(26)-N(2)	1.4375(1.4377)	C(28)-C(29)-C(30)	120.08(120.10)	N(2)-C(26)-C(31)-C(30)	177.13(177.15)
C(26)-C(27)	1.3681(1.3681)	O(1)-C(32)-H(32A)	109.5	N(2)-C(26)-C(27)-C(28)	-176.51(-176.53)
C(26)-C(31)	1.380(1.3840)	O(1)-C(32)-H(32B)	109.5	C(26)-C(27)-C(28)-C(29)	-0.8(-0.9)
C(27)-C(28)	1.3799(1.3810)	O(1)-C(32)-H(32C)	109.5	C(27)-C(28)-C(29)-C(30)	-1.2(-1.4)
C(28)-C(29)	1.377(1.3790)	C(29)-O(1)-C(32)	117.59(117.61)	C(28)-C(29)-C(30)-C(31)	1.9(1.11)
C(30)-C(31)	1.372(1.3730)	O(1)-C(29)-C(28)	123.97(123.99)	C(29)-C(30)-C(31)-C(26)	-0.5(-0.7)
C(29)-C(30)	1.382(1.3840)	O(1)-C(29)-C(30)	115.94(115.95)	C(30)-C(29)-O(1)-C(32)	178.73(178.75)
C(29)-O(1)	1.3696(1.3698)	C(30)-C(31)-C(26)	119.39(119.41)	C(28)-C(29)-O(1)-C(32)	-0.2(-0.4)
C(32)-O(1)	1.423(1.4250)	C(31)-C(30)-C(29)	120.38(120.40)	C(18)-C(19)-C(20)-C(25)	1.1(1.3)
		C(17)-C(16)-C(15)	120.72(120.73)	C(16)-C(17)-C(18)-C(19)	-1.6(-1.8)
		C(25)-C(16)-C(15)	119.17(119.19)	C(23)-C(24)-C(25)-C(16)	-178.90(-178.91)

values in the parenthesis corresponds to theoretical values

Table 3. Photophysical, thermal and electrochemical data of phenanthrimidazoles **1-5**

Compd.	λ_{abs}[a] (nm)	λ_{emi}[a] (nm)	λ_{abs}[b] (nm)	$T_g/T_m/T_{d5}$ (°C)	HOMO[c] (eV)	LUMO[d] (eV)
1	250, 286, 339	422, 367	241	65/262/310	-5.40	-2.32
2	260, 283, 228	423	268	82/265/315	-5.36	-2.37
3	260, 284, 229	435, 363	272	74/248/319	-5.32	-2.36
4	251, 285, 308	414	272	64/272/325	-5.30	-2.38
5	261, 283, 229	409, 365	268	74/261/334	-5.38	-2.35

[a]measured in CH_2Cl_2 solvent at room temperature. [b]solid state. [c]calculated by comparing with ferrocene (Fc) (4.8eV) and calibrated using $E_{1/2}$ (Fc/Fc^+) = 0.22V. [d]HOMO-1239/λ

The electronic spectral studies of naphthyl phenanthrimidazoles have been measured in dichloromethane and the absorption and emission spectra have been displayed in Figure 4. The absorption maxima around 250 nm may originate from aryl ring and the absorption band between 280-339 nm is assigned to $\pi \rightarrow \pi^*$ electronic transition of the phenanthrimidazole ring [63]. Phenanthrimidazole derivatives show emission at 422, 423, 435, 414 and 409 nm, respectively, in CH_2Cl_2.

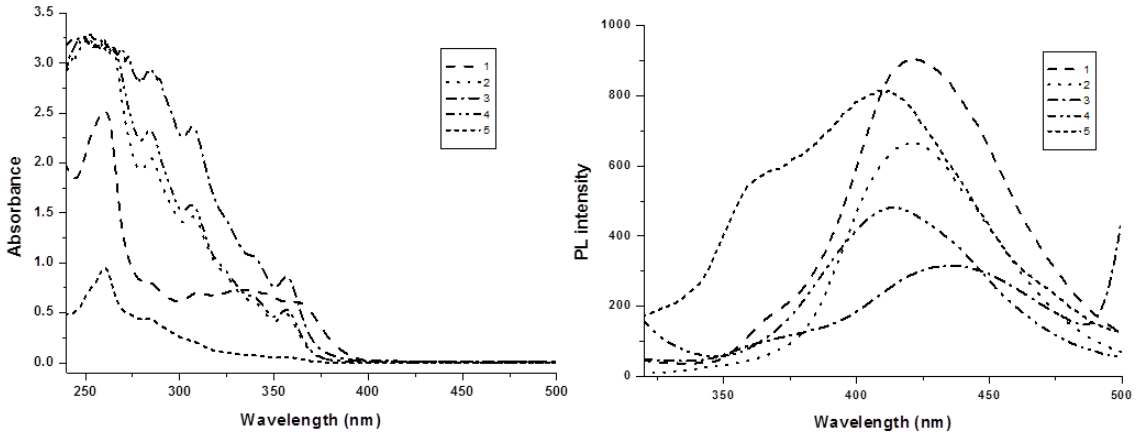

Figure 4. Absorption and emission spectra of phenanthrimidazoles in CH_2Cl_2

The electronic spectra of the phenanthrimidazole materials show remarkable differences in solution and solid state (Figure 5). This may be due to restrained intermolecular

aggregation of bulky and non-coplanar part of these compounds. It can also be correlated to the dihedral parameters of the molecules as shown in Table 4 and the same is given in Figure 5. The red shift can be explained by their stronger π-π stacking interactions due to smaller dihedral angle and the larger dihedral angle results smaller peak shift. The quantum yield (Φ) measured in CH_2Cl_2 solution are, 0.56 (**1**), 0.55 (**2**), 0.53 (**3**), 0.62 (**4**) and 0.59 (**5**). The radiative (k_r) and non-radiative (k_{nr}) decay of the excited state of these compounds have been obtained using the quantum yield and lifetime (τ) and are listed in Table 4. The lifetime decay curve is shown in Figure 6. Radiative lifetime of these compounds fall in the range of 2.09–2.53 ns. Radiative emission of naphthyl phenanthrimidazole derivatives is predominant over non-radiative emission.

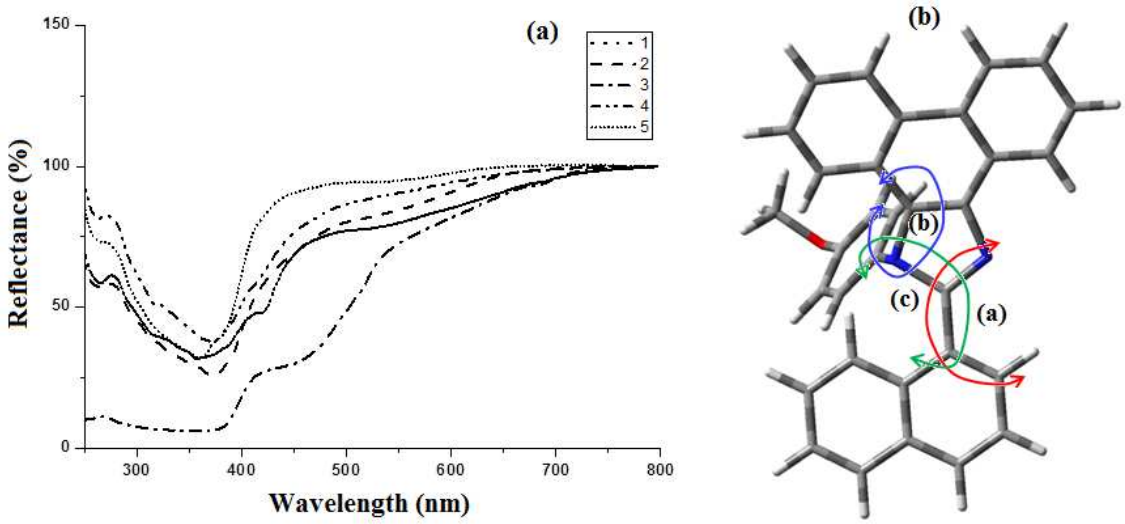

Figure 5. (**a**) Absorption spectra of phenanthrimidazoles in solid state; (**b**) Molecular modeling of phenanthrimidazole using Gaussian-03

DFT calculations show that the methoxy phenenthrimidazole possess larger dihedral angle with the imidazole and naphthyl ring In addition the large dihedral angle between them suppresses the intermolecular π-π stacking in solid state and they prevent self quenching of emission intensity. Examination of quantum yield, radiative (k_r) and non-radiative (k_{nr}) rate constants of the synthesised methoxy phenanthrmidazole exhibit better photophysical properties.

The quantum yield and radiative (k_r) are larger for the methoxy phenanthrmidazole than others and k_{nr} is the least among the studied molecules.

Table 4. Fluorescence quantum yield (Φ), radiative rate constant (k_r, $x10^9$ s^{-1}), non-radiative rate constant (k_{nr}, $x10^9$ s^{-1}) and dihedral angles (°) of phenanthrimidazoles **1-5**

Compd.	Angle[a]	Angle[b]	Angle[c]	Φ	k_r	k_{nr}
1	179	85	74	0.56	0.24	0.19
2	182	154	75	0.55	0.23	0.19
3	174	85	79	0.53	0.21	0.19
4	185	154	118	0.62	0.27	0.16
5	180	86	116	0.59	0.28	0.20

[a]dihedral angle between the imidazole ring and aryl ring; [b]dihedral angle between the imidazole ring and naphthyl ring; [c]dihedral angle between the aryl ring and naphthyl ring

The electrochemical properties of phenanthrimidazoles have been examined by cyclic voltammetry and the redox potentials have been measured from the plot potential *versus* current which is shown in Figure 6. These compounds exhibit one reversible oxidation wave with an oxidation onset potential of 0.60 V (**1**), 0.62 V (**2**), 0.56 V (**3**), 0.50 V (**4**) and 0.58 V (**5**), which gives the HOMO energies of -5.40 eV (**1**), -5.36 eV (**2**), -5.32 eV (**3**), -5.30 eV (**4**) and -5.38 eV (**5**) by comparison to ferrocene ($E_{HOMO} = E_{ox} + 4.8$ eV) [64]. The much smaller HOMO energies support the hole injection ability of these phenanthrimidazoles and the calculated values are displayed in Table 3. The LUMO energies have been deduced from the HOMO energies (Figure 6) and the lowest-energy absorption edges of the UV-vis absorption spectra [64]. The LUMO energies, 2.32 eV (**1**), -2.37 eV (**2**), -2.36 eV (**3**), 2.38 eV (**4**) and -2.35 eV (**5**) are close to that of 1,3,5-tris(N-phenylimidazol-2-yl)benzene (-2.40 eV) revealing that the electron injection abilities of phenanthrimidazoles are similar to 1,3,5-tris(N-phenylimidazol-2-yl)benzene. This reflects the more balanced carrier injection

properties exist in these materials. This result gives us a new direction to introduce new building block emitters by using different substituents to tune the HOMO and LUMO energies [65,66]. To investigate the compounds relationship between structure and properties, their ground-state structure and electronic properties were predicated using B3LYP/6-31G (d, p) level as shown in Figure 6. The electron density of HOMO orbitals are mainly populated on the electron-donating arylamine moieties while the LUMO orbitals are mainly located on electron-accepting phenanthrimidazole moiety. The electron density of HOMO and LUMO orbitals exhibit almost complete separation which is preferable for efficient charge transporting properties [67].

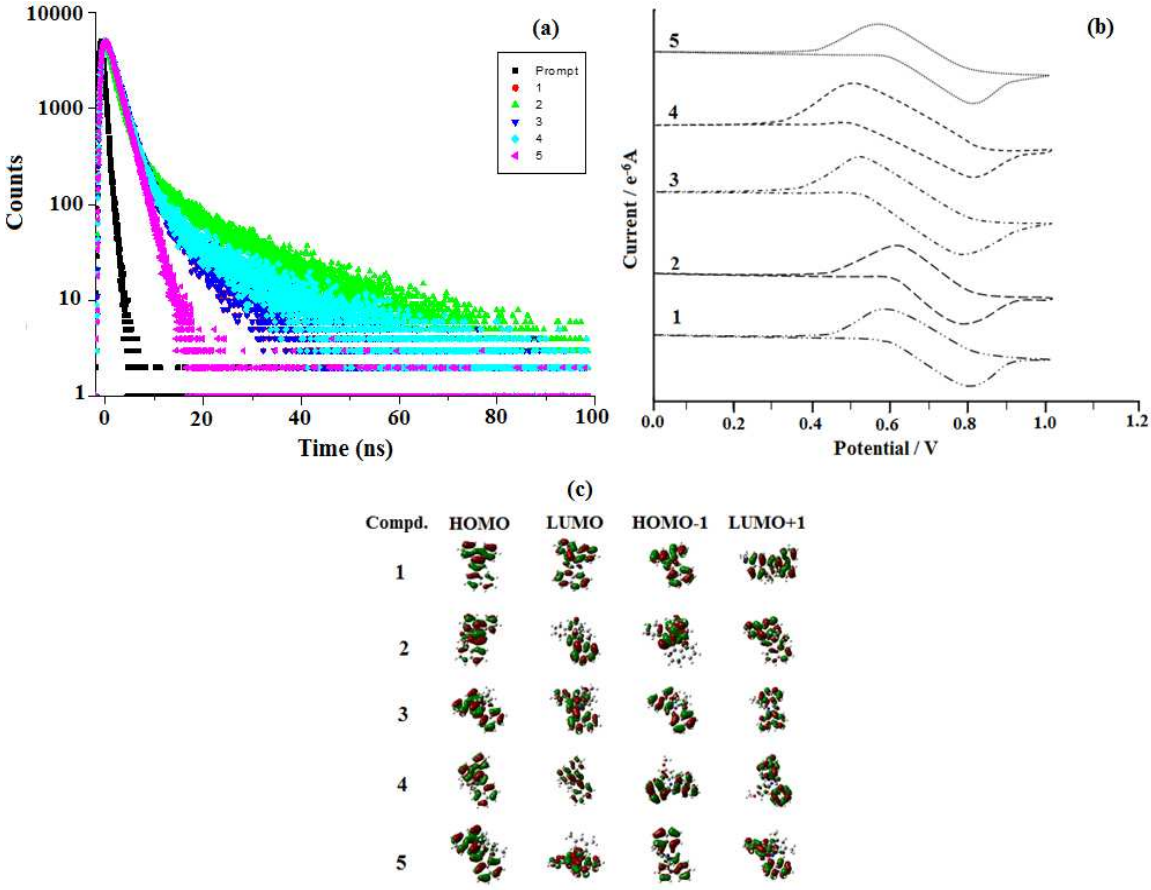

Figure 6. (**a**) Lifetime spectra of naphthyl phenanthrimidazoles **1-5**; (**b**) Cyclic voltammogram of phenanthrimidazoles **1-5**; (**c**) Frontier molecular orbitals of phenanthrimidazoles

Wang et al [63] fabricated OLED with the phenyl substituted phenanthrimidazoles and their results could be compared with the present work in which naphthyl substituted phenanthrimidazoles are used as the functional layer between NPB and ALq_3. The naphthyl substituted phenanthrimidazoles have much shallower HOMO energy than phenyl substituted phenanthrimidazoles (~ -5.58 eV). The shallow HOMO effectively prevents the leakage of holes into the electron transport layer. Attaching naphthyl moiety instead of phenyl to the phenanthrimidazoles play a key role in controlling the HOMO energy levels of the naphthyl phenanthrimidazoles. With the shallow HOMO, it can effectively lower the hole injection barrier from the NPB layer into the phenanthrimidazoles results higher efficiency. Furthermore, the radiative emission of the synthesised naphthyl phenanthrimidazoles is predominant over non-radiative emission. To investigate the EL properties of phenanthrimidazoles, a series of devices (I, II, III, IV and V) with the device configuration of ITO/NPB (10 nm)/**1-5** (30 nm)/Alq_3 (60 nm)/LiF (1 nm)/Al have been fabricated (Figure 7).

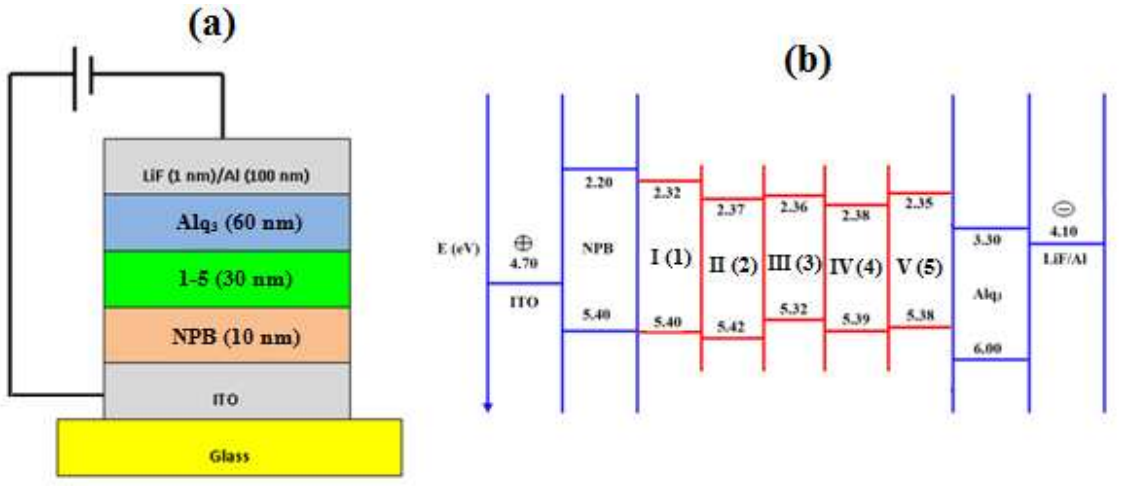

Figure 7. (**a**) General structure of multilayer OLED device; (**b**) Schematic energy level diagram of LUMO/HOMO for devices **I–V**

The devices exhibit emission between 393-431 nm and the current density-brightness-voltage and the luminous efficiencies are listed in Table 5. Figures 8 and 9a & 9b show the

brightness–voltage, power, current efficiencies and the external quantum yield–current density characteristics of the devices, respectively. Devices showed very high brightness and colour stability under different driving voltage. The improved efficiency of devices I–V is due to decrease the leakage of holes through the phenanthrimidazole layer, which results in balancing the electrons and holes in the emitting layer and thus eliminating the non productive hole current.

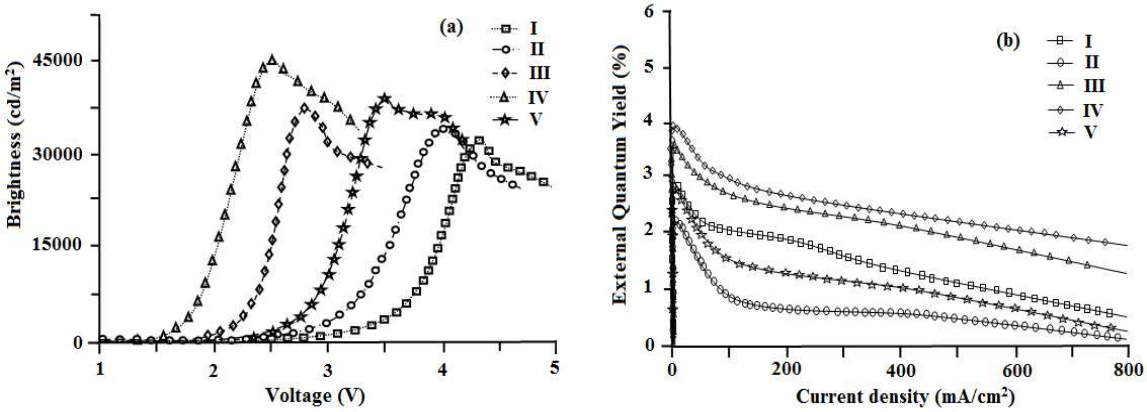

Figure 8. (**a**) Plot of brightness Vs voltage; (**b**) Plot of external quantum yield Vs current density

Table 5. Devices **I-V** based on naphthyl phenanthrimidazoles **1-5**

Device	EL	*V* (V)[a]	L (cd/m^2) [b]	η_{ex} (%)	η_c (cd A^{-1})	η_p (lm W^{-1})
I	431	4.3	31982	2.90	4.01	3.92
II	393	4.0	34129	2.21	4.21	3.81
III	419	2.8	37562	3.56	4.08	3.97
IV	422	2.5	40623	3.92	5.99	5.25
V	409	3.5	38143	2.85	5.41	5.02
VI[63]	-	2.7	37360	-	3.22	-

[a]voltage (*V*) required for 1 cd m^{-12}; [b]The brightness (L) , current efficiency (η_c), external quantum yield(η_{ex} %), power efficiency(η_p)

All devices show quite appreciable efficiencies and brightness. Of the five devices, device II shows poor efficiency followed by devices I and V. The external quantum efficiency of device II is low; even at driven voltage of 4.0, the external quantum efficiency is 2.2 %. The efficiency roll-off may be due to triplet-triplet annihilation [TTA – $_3M^* + {}_3N^* \rightarrow {}_1M + {}_3N^*$] and triplet-polaron annihilation [TPA - $_3M^* + N^- \rightarrow {}_1M + N^{-*}$] as reported in the literature [68]. Baldo *et al.,* [69] reported that triplet-triplet annihilation (TTA) is dominant factor for the external quantum efficiency roll- off. Furthermore, Reineke *et al.,* [70] and Aziz *et al.,* [71] advocated that triplet-polaron annihilation (TPA) could be the only source for efficiency roll-off at high current densities. Simple illustration of these processes is shown in Figure 9c. Though all devices show high efficiencies and brightness, device IV with methoxy phenanthrimidazole shows emission at 422 nm with a maximum current efficiency of 5.99 cd A^{-1}, external quantum efficiency of 3.92 % and a maximum luminance of 40623 cd m^{-2} at a low turn-on voltage of 2.5 V. From the electroluminescent studies it was concluded that the device made from methoxy phenanthrimidazole **4** exhibit a higher device performance which provides the possibility of application in low cost devices. This device performance resulted from its high thermal stability and balanced charge injection properties.

Zhang *et al* [72] reported that incorporation of thiophene at C-2 position of the phenanthrimidazole, namely, 1-(4-tert-butylphenyl)-2-(5-(pyren-1-yl)thiophen-2-yl)-1H-phenanthro[9,10-d]imidazole show maximum brightness of 15960 cd m^{-2} at 4.4 V, current efficiency of 2.93 cd A^{-1}, power efficiency of 3.02 lm w^{-1} and external quantum efficiency of 0.88%. In the present study the reported naphthyl phenanthrimidazole derivatives shows appreciable brightness, external quantum yield, power and current efficiencies when compared with the thiophene substituted phenanthrimidazole derivatives. Comparison of the reference device (VI) with configuration of ITO/NPB (40 nm)/ Alq_3 (60 nm)/LiF (1 nm)/Al

reported by Wang et al [63] show that the current efficiency of the synthesised naphthyl phenanthrimidazoles is higher than the standard one.

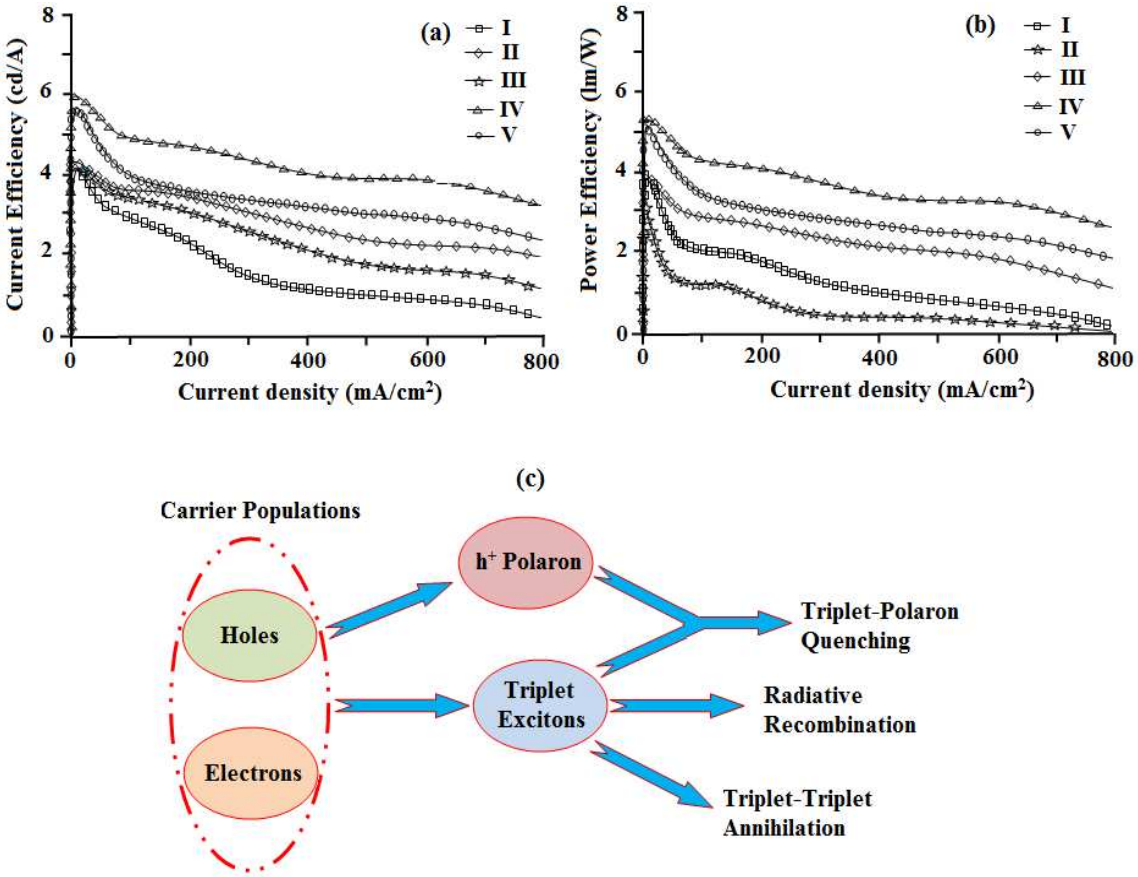

Figure 9. (**a**) Plot of current efficiency Vs current density; (**b**) Plot of power efficiency Vs current density; (**c**) A schematic illustration of TTA and TPA processes

4. Conclusion

Nanocrystalline rutile TiO_2 catalyses the synthesis of naphthyl phenanthrimidazole derivatives under solvent free condition. The high T_m and T_{d5} values indicate that these compounds are thermally stable and can be used to fabricate devices. The naphthyl phenanthrimidazole based devices exhibit higher efficiencies compared with the thiaphene phenanthrimidazoles based devices. Phenanthrimidazoles with shallow HOMO effectively prevent the leakage of holes into the electron transport layer and thus improve the efficiency.

The external quantum efficiency of device II based with 2-(Naphthalen-1-yl)-1-phenyl-1H-phenanthro[9,10-d]imidazole is low when compared with other devices; even at high driven voltage of 4.0, the external quantum efficiency is 2.2 %. The efficiency roll-off may be due to triplet-triplet annihilation [TTA – $_3M^* + {}_3N^* \rightarrow {}_1M + {}_3N^*$] and triplet-polaron annihilation [TPA - $_3M^* + N^- \rightarrow {}_1M + N^{-*}$]. Device based on 1-(4-methoxyphenyl)-2-(naphthalen-1-yl)-1H-phenanthro[9,10-d]imidazole shows brightness of 40623 cd m^{-2}, current efficiency of 5.99 cd A^{-1}, power efficiency of 5.25lmw^{-1} and external quantum efficiency of 3.92 %.

5. Acknowledgments

One of the authors Prof. J. Jayabharathi is thankful to DST [No. SR/S1/IC-73/2010], DRDO (NRB-213/MAT/10-11), UGC (F. No. 36-21/2008 (SR)) and CSIR (NO 3732/NS-EMRII) for providing funds to this research study.

References

[1] N.S. Hush, *Coord. Chem. Rev.,* 1985, **64**, 135-157.

[2] R.A. Marcus, *J. Phys. Chem.,* 1989, **93**, 3078-3086.

[3] I.R. Gould, R.H. Young, R.E. Moody and S. Farid, *J. Phys. Chem.,* 1991, **95**, 2068-2080.

[4] I.R. Gould, D. Noukakis, L. Gomez-Jahn, R.H. Young, J.L. Goodman and S. Farid, *J. Chem. Phys.,* 1993, **176**, 439-456.

[5] J. Cortes, H. Heitele and J. Jortner, *J. Phys. Chem.,* 1994, **98**, 2527-2536.

[6] R.S. Mulliken and W.B. Person, Molecular Complexes: A Lecture and Reprint Volume, VCH, Weinheim, 1969.

[7] J. Nelson, S.A. Haque, D.R. Klug and J.R. Durrant, *Phys. Rev. B.* 2001**, 63**, 205321.

[8] S.E. deLaszlo, C. Hacker, B. Li, D. Kim, M. Maccoss, N. Mantle, J.V. Pivnichny, L. Colwell, G.E. Koch, M.A. Cascieri and W.K. Hagmann, *Bioorg. Med. Chem. Lett.,* 1999, **9**, 641-646.

[9] P.A. Eyers, M. Craxton, N. Morrice, P. Cohen and M. Goedert, *Chem. Biol.,* 1998, **5**, 321–328.

[10] M.J. Newman, J.C. Rodarte, K.D. Benbatoul, S.J. Romano, C. Zhang, S. Krane, E.J. Moran, R.T. Uyeda, R. Dixon, E.S. Guns and L.D. Mayer, *Cancer Res.,* 2000, **60**, 2964-2972.

[11] M. Antolini, A. Bozzoli, C. Ghiron, G. Kennedy, T. Rossi and A. Ursini, *Bioorg. Med. Chem. Lett.,* 1999, **9**, 1023-1028.

[12] J. W. Black, G. J. Durant, J. C. Emmett and C. R. Ganellin, *Nature,* 1974, **248**, 65-67.

[13] Ü. Uçucu, N. G. Karaburun and İ. Işikdağ, *Il Farmaco*, 2001, **56**, 285-290.

[14] L. Wang, K.W. Woods, Q. Li, K.J. Barr, R.W. McCroskey, S.M. Hannick, L. Gherke, R.B. Credo, Y.H. Hui, K. Marsh, R. Warner, J.Y. Lee, N. Zielinski-Mozng, D. Frost, S.H. Rosenberg and H.L. Sham, *J. Med. Chem.,* 2002, **45**, 1697-711.

[15] T. Maier, R. Schmierer, K. Bauer, H. Bieringer, H. Buerstell and B. Sachse, US Patent 4820335, *Chem. Abstr.* 1989, **111**, 1949w.

[16] S.A. Siddiqui, U. C. Narkhede, S. S. Palimkar, T. Daniel, R. J. Lahoti and K. V. Srinivasan, *Tetrahedron*, 2005, **61**, 3539-3546; (b) M. M. Heravi, M. Zakeri, N. Karimi, M. Saeedi, H. A. Oskooie and N. T. Hosieni, *Synth Commun.,* 2010, **40**, 1998-2006.

[17] (a) J. Wang, R. Mason, D. VanDerveer, K. Feng and X.R. Bu, *J. Org. Chem.,* 2003, **68**, 5415-5418; (b) S. Sarshar, D. Siev and M.M Mjalli, *Tetrahedron Lett.*, 1996, **37**, 835-838; (c) T.F. Gallagher, G.L. Seibel, S. Kassis, J.T. Laydon, M.J. Blumenthal, J.C. Lee, D. Lee, J.C. Boehm, S.M. Fier-Thompson, J.W. Abt, M.E. Soreson, J.M. Smietana, R.F. Hall, R.S. Garigipati, P.E. Bender, K.F. Erhard, A.J. Krog, G.A. Hofmann, P.L. Sheldrake, P.C. McDonnell, S. Kumar, P.R. Young and J.L. Adams, *Bioorg. Med. Chem.,* 1997 **5**, 49-64.

[18] A. Shaabani and A. Rahmati, *J. Mol. Catal. A. Chem.,* 2006, **249**, 246-248.

[19] S. Kantevari, S.V.N. Vuppalapati, D. O. Biradar and L. Nagarapu, *J. Mol. Catal. A. Chem.,* 2007, **266**, 109-113.

[20] M. Kidwai, P. Mothsra, V. Babsal and R. Goyal, *Monatsh. Chem.,* 2006, **137**, 1189-1194.

[21] L.M. Wang, Y.H. Wang, H. Tian, Y.F. Yao, J.H. Shao and B. Liu, *J. Fluorine Chem.,* 2006, **127**, 1570-1573.

[22] G.V.M. Sharma, Y. Jyothi and P.S. Lakshmi, *Synth. Commun.,* 2006, **36**, 2991-3000.

[23] S. Balalaie and A. Arabanian, Green Chem., 2000, **2**, 274-276.

[24] M. M. Heravi, K. Bakhtiari, H. A. Oskooie and S. Taheri, *J. Mol. Catal. A. Chem.,* 2007, **263**, 279-281.

[25] K. Sivakumar, A. Kathirvel and A. Lalitha, *Tetrahedron Lett.*, 2010, **51**, 3018-3021.

[26] (a) J. F. Hayes, M. B. Mitchell and C. Wicks, *Heterocycles,* 1994, **38**, 575-585; (b) L. Revesz, F. Bonne and P. Makavou, *Tetrahedron Lett.*, 1998, 39, 5171-5174.

[27] N.J. Liverton, J.W. Butcher, C.F. Claiborne, D.A. Claremon, B.E. Libby, K.T. Nguyen, S. M. Pitzenberger, H.G. Selnick, G.R. Smith, A. Tebben, J. P. Vacca, S. L. Varga, L. Agarwal, K. Dancheck, A.J. Forsyth, D.S. Fletcher, B. Frantz, W.A. Hanlon, C.F. Harper, S.J. Hofsess, M. Kostura, J. Lin, S. Luell, E.A. O'Neill, C. J. Orevillo, M. Pang, J. Parsons, A. Rolando, Y. Sahly, D.M. Visco and S.J. O'Keefe, *J. Med. Chem.*, 1999, **42**, 2180–2190.

[28] U. Diebold, *Surf. Sci. Rep.,* 2003, **48**, 53-229.

[29] D.A Tryk, A Fujishima and K Honda, *Electrochimica Acta.*, 2000, **45**, 2363-2376.

[30] L. G. Phillips and D. M. Barbano, *J. Dairy Sci.,* 1997, **80**, 2726-2731.

[31] J.P. Hewitt, *Cosmet. Toiletries,* 1999, **114***,* 59-63.

[32]G. Palmisano, V. Augugliaro, M. Pagliaro and L. Palmisano, *Chem. Commun.*, 2007, 3425-3437.

[33] M. Mahalakshmi, Banumathi Arabindoo, M. Palanichamy and V. Murugesan, *J. Hazard. Mater.,* 2007, **143**, 240-245.

[34] M. Abu Tariq, M. Faisal and M. Muneer, *J. Hazard. Mater.,* 2005, **127,** 172-179.

[35] O. S. Mohamed, A.E-A.M. Gaber and A.A. Abdel-Wahab, *J. Photochem. Photobiol. A.* 2002, **148**, 205-210.

[36] H. Sharghi and M. Hosseini Sarvari, *J. Chem. Res. (S),* **2003**, 176.

[37] M.A. Pasha, K. Manjula and V.P. Jayashankara, *Synth. React. Inorg. Met.-Org. Chem.,* 2006, **36**, 321-324.

[38] M. Z. Kassaee, H. Masrouri, F. Movahedi and R. Mohammadi, *Helv. Chim. Acta.,* 2010, **93**, 261-264.

[39] K. V. Subba Rao, B. Srinivas, A. R. Prasad and M. Subrahmanyam, *Chem. Commun.*, 2000, 1533-1534.

[40] K. V. Subba Rao and M. Subrahmanyam, *Photochem. Photobiol. Sci.*, 2002, **1**, 597-599.

[41] V. Jeena and R. S. Robinson, *Beilstein J. Org. Chem.* 2009, **5***,* No. 24. doi:10.3762/bjoc.5.24.

[42] X. J. Lang; H. W. Ji; C. C. Chen; W. H. Ma; J. C. Zhao**,** *Angew. Chem. Int. Ed.*, 2011, **50**, 3934-3937.

[43] (a) C. W. Tang and S. A. Vanslyke, *Appl. Phys. Lett.,* 1987, **51**, 913-915; (b) C. W. Tang, S. A. Vanskyke and C. H. Chen, *J. Appl. Phys.,* 1989, **65**, 3610-3616.

[44] (a) M. A. Baldo, D. F. O'Brien, Y. You, A. Shoustikov, S. Sibley, M. E. Thompson and S. R. Forrest, *Nature,* 1998, **395**, 151-154; (b) X. H. Zhang, B. J. Chen, X. Q. Lin, O. Y. Wong, C. S. Lee, H. L. Kwong, S. T. Lee and S. K. Wu, *Chem. Mater.,* 2001, **13**, 1565-1569; (c) K. Q. Ye, J. Wang, H. Sun, Y. Liu, Z. C. Mu, F. Li, S. M. Jiang, J. Y. Zhang, H. X. Zhang, Y. Wang and C. M. Che, *J. Phys. Chem. B.,* 2005, **109**, 8008-8016; (d) H. Bi, K. Q. Ye, Y. F. Zhao, Y. Yang, Y. Liu and Y. Wang, *Org. Electron.,* 2010, **11**, 1180-1184.

[45] L. S. Hung and C. H. Chen, *Mater. Sci. Eng., R.* 2002, **39**, 143-222.

[46] (a) G. G. Malliaras, Y. Shen, D. H. Dunlap, H. Murata and Z. H. Kafafi, *Appl. Phys. Lett.,* 2001, **79**, 2582-2584; (b) S. C. Tse, H. H. Fong and S. K. So, *J. Appl. Phys.,* 2003, **94**, 2033-2037; (c) S. C. Tse, S. K. So, M. Y. Yeung, C. F. Lo, S. W. Wen and C. H. Chen, *Jpn. J. Appl. Phys.,* 2006, **45**, 555.

[47] (a) S. C. Tse, K. C. Kwok and S. K. So, *Appl. Phys. Lett.,* 2006, **89**, 262102-3; (b) K. K. Tsung and S. K. So, *Appl. Phys. Lett.,* 2008, **92**, 103315-3.

[48] (a) Y. Shirota, Y. Kuwabara, H. Inada, T. Wakimoto, H. Nakada, Y. Yonemoto, S. Kawami and K. Imai, *Appl. Phys. Lett.,* 1994, **65**, 807; (b) S. A. VanSlyke, C. H. Chen

and C. W. Tang, *Appl. Phys. Lett.,* 1996, **69**, 2160-2162; (c) S. A. Carter, M. Angelopoulos, S. Karg, P. J. Brock and J. C. Scott, *Appl. Phys. Lett.,* 1997, **70**, 2067-2069.

[49] (a) Z. B. Deng, X. M. Ding, S. T. Lee and W. A. Gambling, *Appl. Phys. Lett.,* 1999, **74**, 2227-2229; (b) H. J. Jiang, Y. Zhou, B. S. Ooi, Y. W. Chen, T. Wee, Y. L. Lam, J. S. Huang and S. Y. Liu, *Thin Solid Films,* 2000, **363**, 25-28; (c) C. F. Qiu, H. Y. Chen, Z. L. Xie, M. Wong and H. S. Kwok, *Appl. Phys. Lett.,* 2002, **80**, 3485-3487; (d) Y. Kurosaka, N. Tada, Y. Ohmori and K. Yoshino, *Synth. Met.,* 1999, **102**, 1101-1102; (e) I. M. Chan, T. Y. Hsu and E. C. Hong, *Appl. Phys. Lett.,* 2002, **81**, 1899-1901; (f) W. P. Hu, M. Matsumura, K. Furukawa and K. Torimitsu, *J. Phys. Chem. B.,* 2004, **108**, 13116-13118.

[50] (a) J. Kwon, T. H. Kwon, H. S. Cho, M. K. Kim, I. S. Shin, D. Y. Shin, S. J. Park and J. I. Hong, *New J. Chem.,* 2008, **32**, 1368-1372; (b) L. Aubouy, N. Huby, L. Hirsch, A. van der Lee and P. Gerbier, *New J. Chem.,* 2009, **33**, 1290-1300.

[51] (a) J. Jayabharathi, V. Thanikachalam, V. Kalaiarasi and K. Jayamoorthy, *J. Photochem. Photobiol., A.* 2014, **275**, 114-126; (b) J. Jayabharathi, V. Thanikachalam, V. Kalaiarasi and K. Jayamoorthy, *Spectrochim. Acta, Part A.* 2014, **120**, 389-394; (c) C. Karunakaran, J. Jayabharathi, V. Kalaiarasi and K. Jayamoorthy, *Spectrochim.Acta, Part A.* 2014, **118**, 182-186; (d) J. Jayabharathi, V. Kalaiarasi, V. Thanikachalam and K. Jayamoorthy, *J. Fluoresc.,* 2014, **24**, 625-637; (e) J. Jayabharathi, V. Thanikachalam, P. Ramanathan and A. Arunpandiyan, *Spectrochim. Acta, Part A.* 2014, **121**, 551-558; (f) J. Jayabharathi, P. Ramanathan, V. Thanikachalam and A. Arunpandiyan, *Spectrochim. Acta, Part A.* 2014, **133**, 201-206; (g) J. Jayabharathi, C. Karunakaran, V. Thanikachalam and P. Ramanathan, *New J. Chem.,* 2014, **38**, 4321-4335; (h) V. Thanikachalam, A. Arunpandiyan, J. Jayabharathi and P. Ramanathan,

RSC adv., 2014, **4**, 6790-6806; (i) V. Thanikachalam, J. Jayabharathi, A. Arunpandiyan and P. Ramanathan, *J. Fluoresc.,* 2014, **24**, 377-387.

[52] I. Yoshikatsu and M. Teruo, *J. Org. Chem.,* 1979, **44**, 41-49.

[53] J. Nikkanen, T. Kanerva, T. Ma¨ntyla, *J. Cryst. Growth.,* 2007, **304**, 179-183.

[54] H. Cheng, J. Ma, Z. Zhao and L. Qi, *Chem. Mater.,* 1995, **7***,* 663-671.

[55] J. Jayabharathi, V. Thanikachalam and K. Saravanan, *J. Photochem. Photobiol. A.* 2009, **208**, 13-20.

[56] J. Jayabharathi, V. Thanikachalam, M. Venkatesh Perumal and N. Srinivasan, *Spectrochim.Acta, Part A.* 2011, **79**, 236-244.

[57] S. Okada, K. Okinaka, H. Iwawaki, M. Furugori, M. Hashimoto, T. Mukaide, J. Kamatani, S. Igawa, A. Tsuboyama, T. Takiguchi and K. Ueno, *Dalton Trans.,* 2005, **9**, 1583-1590.

[58] M. J. Frisch, G. W. Trucks, H. B. Schlegel, G. E. Scuseria, M. A. Robb, J. R. Cheeseman, J. A. Montgomery, Jr., T. Vreven, K. N. Kudin, J. C. Burant, J. M. Millam, S. S. Iyengar, J. Tomasi, V. Barone, B. Mennucci, M. Cossi, G. Scalmani, N. Rega, G. A. Petersson, H. Nakatsuji, M. Hada, M. Ehara, K. Toyota, R. Fukuda, J. Hasegawa, M. Ishida, T. Nakajima, Y. Honda, O. Kitao, H. Nakai, M. Klene, X. Li, J. E. Knox, H. P. Hratchian, J. B. Cross, V. Bakken, C. Adamo, J. Jaramillo, R. Gomperts, R. E. Stratmann, O. Yazyev, A. J. Austin, R. Cammi, C. Pomelli, J. W. Ochterski, P. Y. Ayala, K. Morokuma, G. A. Voth, P. Salvador, J. J. Dannenberg, V. G. Zakrzewski, S. Dapprich, A. D. Daniels, M. C. Strain, O. Farkas, D. K. Malick, A. D. Rabuck, K. Raghavachari, J. B. Foresman, J. V. Ortiz, Q. Cui, A. G. Baboul, S. Clifford, J. Cioslowski, B. B. Stefanov, G. Liu, A. Liashenko, P. Piskorz, I. Komaromi, R. L. Martin, D. J. Fox, T. Keith, M. A. Al-Laham, C. Y. Peng, A. Nanayakkara, M.

Challacombe, P. M. W. Gill, B. Johnson, W. Chen, M. W. Wong, C. Gonzalez, J. A. Pople, Gaussian 03 (Revision E.01), Gaussian, Inc., Wallingford, CT, 2004.

[59] C. Karunakaran and P. Gomathisankar, *ACS Sustainable Chem. Eng.,* 2003, **1**, 1549-1555.

[60] M. Veeranarayana Reddy and Y. T. Jeong, *J. Fluorine Chem.,* 2012, **142**, 45-51.

[61] A. Wakamiya, T. Taniguchi and S. Yamaguchi, *Angew. Chem.,* 2006, **118**, 3242-3245.

[62] C. Fan, Y. H. Chen, Z. Q. Jiang, C. L. Yang, C. Zhong, J. G. Qin and D. G. Ma, *J. Mater. Chem.,* 2010, **20**, 3232-3237.

[63] Y. Yuan, D. Li, X. Zhang, X. Zhao, Y. Liu, J. Zhang and Y. Wang, *New. J. Chem.,* 2011, **35**, 1534-1540.

[64] (a) S. Ranjan, S.Y. Lin, K.C. Hwang, Y. Chi, W.L. Ching, C.S. Liu, Y.T. Tao, C.H. Chien, S.M. Peng and G.H. Lee, *Inorg. Chem.,* 2003, **42**, 1248-1255; (b) S.L. Lin, L.H. Chan, R.H. Lee, M.Y. Yen, W.J. Kuo, C.T. Chen and R.J. Jeng, *Adv. Mater.,* 2008, **20**, 3947-3952.

[65] (a) A. P. Kulkarni, A. P. Gifford, C. J. Tonzola and S. A. Jenekhe, *Appl. Phys. Lett.,* 2005, **86**, 061106-3; (b) W. L. Yu, J. Pei, Y. Cao and W. Huang, *J. Appl. Phys.,* 2001, **89**, 2343-2350.

[66] (a) J. Staudigel, M. Stossel, F. Steuber and J. Simmerer, *J. Appl. Phys.,* 1999, **86**, 3895-3910; (b) Y. Kawabe and J. Abe, *Appl. Phys. Lett.,* 2002, **81**, 493-495; (c) M.T. Lee, H. H. Chen, C. H. Liao, C. H. Tsai and C. H. Chen, *Appl. Phys. Lett.,* 2004, **85**, 3301-3303; (d) Q. X. Tong, S. L. Lai, M.Y. Chan, Y. C. Zhou, H. L. Kwong, C. S. Lee and S.T. Lee, *J. Phys. Chem. C.,* 2009, **113**, 6227-6230.

[67] Y. Tao, Q. Wang, C. Yang, C. Zhong, K. Zhang, J. Qin and D. Ma, *Adv. Funct. Mater.,* 2010, **20**, 304-311.

[68] (a) Q. Wang, I. W. H. Oswald, M. R. Perez, H. Jia, A. A. Shahub, Q. Qiao, B. E. Gnade and M.A. Omary, *Adv. Funct. Mater*., 2014, **24**, 4746-4752; (b) Q. Wang, I. W. H. Oswald, M. R. Perez, H. P. Jia, B. E. Gnade and M. A. Omary, *Adv. Funct. Mater.,* 2013, **23**, 5420 -5428; (c) C. Fan and C. Yang, *Chem. Soc. Rev.,* 2010, **39**, 2387-2398; (d) Q. Wang, J. Ding, D. Ma, Y. Cheng, L. Wang, X. Jing and F. Wang, *Adv. Funct. Mater.,* 2009, **19**, 84-95; (e) B. Q. Wang, J. Ding, D. Ma, Y. Cheng, L. Wang and F. Wang, *Adv. Mater.,* 2009, **21**, 2397-2401.

[69] M. A. Baldo , C. Adachi and S. R. Forrest, *Phys. Rev., B.* 2000, **62**, 10967.

[70] S. Reineke, K. Walzer, and K. Leo, *Phys. Rev.,* B. 2007, **75**, 125328.

[71] D. Song, S. Zhao, Y. Luo and H. Aziz, *Appl. Phys. Lett*., 2010, **97**, 243304.

[72] Y. Zhang, S.L. Lai, Q.X. Tong, M.Y. Chan, T.W. Ng, Z.C. Wen, G.Q. Zhang, S.T. Lee, H.L. Kwonge and C.S. Lee, *J. Mater. Chem.,* 2011, **21**, 8206-8214.

Table 1. Crystal data and structure refinement for pr4.

Identification code	shelxl
Empirical formula	C32 H22 N2 O
Formula weight	450.52
Temperature	293(2) K
Wavelength	0.71073 A
Crystal system, space group	Monoclinic, P21/c
Unit cell dimensions	a = 12.3316(7) A alpha = 90 deg. b = 21.3475(11) A beta = 92.340(3) deg. c = 8.8212(5) A gamma = 90 deg.
Volume	2320.2(2) A^3
Z, Calculated density	4, 1.290 Mg/m^3
Absorption coefficient	0.078 mm^-1
F(000)	944
Crystal size	0.35 x 0.30 x 0.25 mm
Theta range for data collection	2.50 to 30.64 deg.
Limiting indices	-17<=h<=17, -28<=k<=30, -12<=l<=12
Reflections collected / unique	29016 / 7155 [R(int) = 0.0401]
Completeness to theta = 30.64	99.8 %
Absorption correction	Semi-empirical from equivalents
Max. and min. transmission	0.9807 and 0.9232
Refinement method	Full-matrix least-squares on F^2
Data / restraints / parameters	7155 / 0 / 317
Goodness-of-fit on F^2	1.024
Final R indices [I>2sigma(I)]	R1 = 0.0528, wR2 = 0.1186
R indices (all data)	R1 = 0.1092, wR2 = 0.1422
Largest diff. peak and hole	0.170 and -0.212 e.A^-3

Table 2. Atomic coordinates (x 10^4) and equivalent isotropic displacement parameters (A^2 x 10^3) for pr4.
U(eq) is defined as one third of the trace of the orthogonalized Uij tensor.

	x	y	z	U(eq)
C(1)	1654(1)	4554(1)	2458(2)	39(1)
C(2)	1640(1)	4081(1)	1312(2)	40(1)
C(3)	982(1)	4123(1)	-15(2)	50(1)
C(4)	1046(1)	3682(1)	-1125(2)	58(1)
C(5)	1750(1)	3179(1)	-931(2)	60(1)
C(6)	2372(1)	3119(1)	376(2)	53(1)
C(7)	2346(1)	3565(1)	1541(2)	42(1)
C(8)	3034(1)	3519(1)	2930(2)	41(1)
C(9)	3779(1)	3025(1)	3160(2)	51(1)
C(10)	4436(1)	2982(1)	4445(2)	56(1)
C(11)	4355(1)	3419(1)	5585(2)	55(1)
C(12)	3642(1)	3906(1)	5420(2)	49(1)
C(13)	2995(1)	3979(1)	4086(2)	40(1)
C(14)	2295(1)	4503(1)	3763(2)	38(1)
C(15)	1398(1)	5400(1)	3680(2)	40(1)
C(16)	1084(1)	6041(1)	4120(2)	42(1)
C(17)	248(1)	6137(1)	5057(2)	57(1)
C(18)	-77(2)	6742(1)	5428(2)	73(1)
C(19)	452(2)	7245(1)	4889(2)	71(1)
C(20)	1333(1)	7174(1)	3941(2)	53(1)
C(21)	1912(2)	7690(1)	3382(2)	71(1)
C(22)	2749(2)	7607(1)	2459(2)	75(1)
C(23)	3050(2)	7005(1)	2037(2)	68(1)
C(24)	2521(1)	6492(1)	2551(2)	52(1)
C(25)	1652(1)	6560(1)	3529(2)	42(1)
C(26)	2632(1)	5255(1)	5967(2)	39(1)
C(27)	3666(1)	5487(1)	5972(2)	47(1)
C(28)	4200(1)	5653(1)	7318(2)	49(1)
C(29)	3676(1)	5589(1)	8658(2)	46(1)
C(30)	2620(1)	5373(1)	8645(2)	56(1)
C(31)	2096(1)	5203(1)	7305(2)	50(1)
C(32)	5238(1)	5931(1)	10120(2)	74(1)
N(1)	1092(1)	5114(1)	2416(1)	44(1)
N(2)	2117(1)	5053(1)	4559(1)	40(1)
O(1)	4144(1)	5719(1)	10058(1)	67(1)

Table 3. Bond lengths [A] and angles [deg] for pr4.

C(1)-C(14)	1.3744(18)
C(1)-N(1)	1.3809(16)
C(1)-C(2)	1.4279(18)
C(2)-C(3)	1.3998(19)
C(2)-C(7)	1.4142(19)
C(3)-C(4)	1.363(2)
C(3)-H(3)	0.9300
C(4)-C(5)	1.386(2)
C(4)-H(4)	0.9300
C(5)-C(6)	1.364(2)
C(5)-H(5)	0.9300
C(6)-C(7)	1.4025(19)
C(6)-H(6)	0.9300
C(7)-C(8)	1.4649(19)
C(8)-C(9)	1.4073(19)
C(8)-C(13)	1.4180(19)
C(9)-C(10)	1.370(2)
C(9)-H(9)	0.9300
C(10)-C(11)	1.378(2)
C(10)-H(10)	0.9300
C(11)-C(12)	1.366(2)
C(11)-H(11)	0.9300
C(12)-C(13)	1.4028(19)
C(12)-H(12)	0.9300
C(13)-C(14)	1.4349(18)
C(14)-N(2)	1.3897(16)
C(15)-N(1)	1.3132(17)
C(15)-N(2)	1.3710(17)
C(15)-C(16)	1.4779(18)
C(16)-C(17)	1.363(2)
C(16)-C(25)	1.4214(19)
C(17)-C(18)	1.395(2)
C(17)-H(17)	0.9300
C(18)-C(19)	1.353(3)
C(18)-H(18)	0.9300
C(19)-C(20)	1.405(2)
C(19)-H(19)	0.9300
C(20)-C(21)	1.413(2)
C(20)-C(25)	1.4195(19)
C(21)-C(22)	1.352(3)
C(21)-H(21)	0.9300
C(22)-C(23)	1.393(2)
C(22)-H(22)	0.9300
C(23)-C(24)	1.360(2)
C(23)-H(23)	0.9300
C(24)-C(25)	1.411(2)
C(24)-H(24)	0.9300
C(26)-C(27)	1.3681(19)
C(26)-C(31)	1.380(2)
C(26)-N(2)	1.4375(16)
C(27)-C(28)	1.3799(19)
C(27)-H(27)	0.9300
C(28)-C(29)	1.377(2)
C(28)-H(28)	0.9300
C(29)-O(1)	1.3696(16)
C(29)-C(30)	1.382(2)

C(30)-C(31)	1.372(2)
C(30)-H(30)	0.9300
C(31)-H(31)	0.9300
C(32)-O(1)	1.423(2)
C(32)-H(32A)	0.9600
C(32)-H(32B)	0.9600
C(32)-H(32C)	0.9600

C(14)-C(1)-N(1)	111.22(11)
C(14)-C(1)-C(2)	121.82(12)
N(1)-C(1)-C(2)	126.92(12)
C(3)-C(2)-C(7)	120.12(13)
C(3)-C(2)-C(1)	122.49(12)
C(7)-C(2)-C(1)	117.38(12)
C(4)-C(3)-C(2)	120.54(14)
C(4)-C(3)-H(3)	119.7
C(2)-C(3)-H(3)	119.7
C(3)-C(4)-C(5)	120.03(15)
C(3)-C(4)-H(4)	120.0
C(5)-C(4)-H(4)	120.0
C(6)-C(5)-C(4)	120.31(15)
C(6)-C(5)-H(5)	119.8
C(4)-C(5)-H(5)	119.8
C(5)-C(6)-C(7)	121.81(14)
C(5)-C(6)-H(6)	119.1
C(7)-C(6)-H(6)	119.1
C(6)-C(7)-C(2)	117.13(13)
C(6)-C(7)-C(8)	122.54(13)
C(2)-C(7)-C(8)	120.30(12)
C(9)-C(8)-C(13)	117.15(13)
C(9)-C(8)-C(7)	121.55(13)
C(13)-C(8)-C(7)	121.28(12)
C(10)-C(9)-C(8)	122.04(15)
C(10)-C(9)-H(9)	119.0
C(8)-C(9)-H(9)	119.0
C(9)-C(10)-C(11)	119.98(14)
C(9)-C(10)-H(10)	120.0
C(11)-C(10)-H(10)	120.0
C(12)-C(11)-C(10)	120.25(15)
C(12)-C(11)-H(11)	119.9
C(10)-C(11)-H(11)	119.9
C(11)-C(12)-C(13)	121.00(14)
C(11)-C(12)-H(12)	119.5
C(13)-C(12)-H(12)	119.5
C(12)-C(13)-C(8)	119.45(12)
C(12)-C(13)-C(14)	124.72(12)
C(8)-C(13)-C(14)	115.81(12)
C(1)-C(14)-N(2)	105.01(11)
C(1)-C(14)-C(13)	123.28(12)
N(2)-C(14)-C(13)	131.68(12)
N(1)-C(15)-N(2)	112.69(12)
N(1)-C(15)-C(16)	125.77(12)
N(2)-C(15)-C(16)	121.43(12)
C(17)-C(16)-C(25)	120.09(13)
C(17)-C(16)-C(15)	120.72(13)
C(25)-C(16)-C(15)	119.17(12)
C(16)-C(17)-C(18)	120.86(15)
C(16)-C(17)-H(17)	119.6
C(18)-C(17)-H(17)	119.6
C(19)-C(18)-C(17)	120.34(16)

C(19)-C(18)-H(18)	119.8
C(17)-C(18)-H(18)	119.8
C(18)-C(19)-C(20)	121.23(15)
C(18)-C(19)-H(19)	119.4
C(20)-C(19)-H(19)	119.4
C(19)-C(20)-C(21)	122.48(15)
C(19)-C(20)-C(25)	118.78(14)
C(21)-C(20)-C(25)	118.75(15)
C(22)-C(21)-C(20)	121.17(16)
C(22)-C(21)-H(21)	119.4
C(20)-C(21)-H(21)	119.4
C(21)-C(22)-C(23)	119.98(17)
C(21)-C(22)-H(22)	120.0
C(23)-C(22)-H(22)	120.0
C(24)-C(23)-C(22)	121.09(17)
C(24)-C(23)-H(23)	119.5
C(22)-C(23)-H(23)	119.5
C(23)-C(24)-C(25)	120.57(15)
C(23)-C(24)-H(24)	119.7
C(25)-C(24)-H(24)	119.7
C(24)-C(25)-C(20)	118.44(13)
C(24)-C(25)-C(16)	122.89(13)
C(20)-C(25)-C(16)	118.67(13)
C(27)-C(26)-C(31)	120.31(13)
C(27)-C(26)-N(2)	119.36(12)
C(31)-C(26)-N(2)	120.32(12)
C(26)-C(27)-C(28)	120.55(13)
C(26)-C(27)-H(27)	119.7
C(28)-C(27)-H(27)	119.7
C(29)-C(28)-C(27)	119.24(13)
C(29)-C(28)-H(28)	120.4
C(27)-C(28)-H(28)	120.4
O(1)-C(29)-C(28)	123.97(13)
O(1)-C(29)-C(30)	115.94(13)
C(28)-C(29)-C(30)	120.08(13)
C(31)-C(30)-C(29)	120.38(13)
C(31)-C(30)-H(30)	119.8
C(29)-C(30)-H(30)	119.8
C(30)-C(31)-C(26)	119.39(13)
C(30)-C(31)-H(31)	120.3
C(26)-C(31)-H(31)	120.3
O(1)-C(32)-H(32A)	109.5
O(1)-C(32)-H(32B)	109.5
H(32A)-C(32)-H(32B)	109.5
O(1)-C(32)-H(32C)	109.5
H(32A)-C(32)-H(32C)	109.5
H(32B)-C(32)-H(32C)	109.5
C(15)-N(1)-C(1)	104.66(11)
C(15)-N(2)-C(14)	106.41(11)
C(15)-N(2)-C(26)	125.40(11)
C(14)-N(2)-C(26)	128.04(11)
C(29)-O(1)-C(32)	117.59(12)

Symmetry transformations used to generate equivalent atoms:

Table 4. Anisotropic displacement parameters (A^2 x 10^3) for pr4.
The anisotropic displacement factor exponent takes the form:
-2 pi^2 [h^2 a*^2 U11 + ... + 2 h k a* b* U12]

	U11	U22	U33	U23	U13	U12
C(1)	38(1)	39(1)	40(1)	2(1)	2(1)	-2(1)
C(2)	41(1)	40(1)	40(1)	0(1)	4(1)	-6(1)
C(3)	54(1)	47(1)	48(1)	1(1)	-7(1)	-3(1)
C(4)	66(1)	59(1)	48(1)	-5(1)	-10(1)	-12(1)
C(5)	68(1)	56(1)	55(1)	-15(1)	1(1)	-10(1)
C(6)	55(1)	48(1)	57(1)	-10(1)	5(1)	-1(1)
C(7)	40(1)	43(1)	43(1)	-2(1)	7(1)	-6(1)
C(8)	38(1)	40(1)	46(1)	2(1)	7(1)	-2(1)
C(9)	54(1)	44(1)	56(1)	1(1)	10(1)	4(1)
C(10)	51(1)	50(1)	66(1)	10(1)	4(1)	12(1)
C(11)	55(1)	54(1)	56(1)	11(1)	-7(1)	4(1)
C(12)	51(1)	48(1)	47(1)	3(1)	-3(1)	2(1)
C(13)	36(1)	41(1)	42(1)	3(1)	2(1)	-2(1)
C(14)	37(1)	39(1)	37(1)	0(1)	3(1)	-3(1)
C(15)	38(1)	41(1)	41(1)	1(1)	2(1)	0(1)
C(16)	41(1)	45(1)	40(1)	-2(1)	-3(1)	3(1)
C(17)	54(1)	58(1)	61(1)	-3(1)	14(1)	-1(1)
C(18)	67(1)	72(1)	81(1)	-14(1)	27(1)	9(1)
C(19)	75(1)	54(1)	85(1)	-18(1)	13(1)	13(1)
C(20)	55(1)	46(1)	58(1)	-6(1)	-3(1)	2(1)
C(21)	85(1)	44(1)	83(1)	-2(1)	-4(1)	-3(1)
C(22)	82(1)	58(1)	86(1)	13(1)	7(1)	-17(1)
C(23)	62(1)	71(1)	73(1)	10(1)	14(1)	-8(1)
C(24)	51(1)	51(1)	55(1)	2(1)	6(1)	2(1)
C(25)	42(1)	44(1)	41(1)	-1(1)	-4(1)	3(1)
C(26)	41(1)	40(1)	37(1)	-1(1)	0(1)	-2(1)
C(27)	45(1)	58(1)	38(1)	0(1)	6(1)	-9(1)
C(28)	42(1)	59(1)	45(1)	-3(1)	2(1)	-13(1)
C(29)	51(1)	51(1)	37(1)	-4(1)	-2(1)	-4(1)
C(30)	54(1)	77(1)	37(1)	-2(1)	11(1)	-12(1)
C(31)	41(1)	63(1)	45(1)	-1(1)	6(1)	-11(1)
C(32)	64(1)	95(1)	61(1)	-14(1)	-16(1)	-16(1)
N(1)	45(1)	42(1)	44(1)	-1(1)	-4(1)	1(1)
N(2)	39(1)	42(1)	38(1)	-2(1)	0(1)	-1(1)
O(1)	64(1)	94(1)	41(1)	-11(1)	-2(1)	-17(1)

Table 5. Hydrogen coordinates (x 10^4) and isotropic displacement parameters (A^2 x 10^3) for pr4.

	x	y	z	U(eq)
H(3)	497	4454	-141	60
H(4)	617	3718	-2013	69
H(5)	1799	2882	-1695	72
H(6)	2825	2773	497	63
H(9)	3827	2719	2415	61
H(10)	4937	2657	4549	67
H(11)	4787	3382	6469	66
H(12)	3584	4194	6204	59
H(17)	-111	5795	5455	69
H(18)	-660	6800	6049	87
H(19)	229	7645	5150	85
H(21)	1714	8094	3654	85
H(22)	3124	7952	2106	90
H(23)	3621	6952	1393	82
H(24)	2735	6095	2256	63
H(27)	4011	5534	5061	56
H(28)	4906	5806	7319	58
H(30)	2261	5342	9549	67
H(31)	1387	5055	7298	60
H(32A)	5687	5630	9635	111
H(32B)	5484	5979	11160	111
H(32C)	5283	6326	9607	111

Table 6. Torsion angles [deg] for pr4.

C(14)-C(1)-C(2)-C(3)	179.25(13)
N(1)-C(1)-C(2)-C(3)	-3.2(2)
C(14)-C(1)-C(2)-C(7)	-2.35(19)
N(1)-C(1)-C(2)-C(7)	175.17(12)
C(7)-C(2)-C(3)-C(4)	-2.7(2)
C(1)-C(2)-C(3)-C(4)	175.66(13)
C(2)-C(3)-C(4)-C(5)	1.4(2)
C(3)-C(4)-C(5)-C(6)	0.8(2)
C(4)-C(5)-C(6)-C(7)	-1.7(2)
C(5)-C(6)-C(7)-C(2)	0.4(2)
C(5)-C(6)-C(7)-C(8)	-177.93(14)
C(3)-C(2)-C(7)-C(6)	1.77(19)
C(1)-C(2)-C(7)-C(6)	-176.67(12)
C(3)-C(2)-C(7)-C(8)	-179.86(12)
C(1)-C(2)-C(7)-C(8)	1.71(18)
C(6)-C(7)-C(8)-C(9)	1.1(2)
C(2)-C(7)-C(8)-C(9)	-177.15(13)
C(6)-C(7)-C(8)-C(13)	179.65(13)
C(2)-C(7)-C(8)-C(13)	1.36(19)
C(13)-C(8)-C(9)-C(10)	0.6(2)
C(7)-C(8)-C(9)-C(10)	179.18(13)
C(8)-C(9)-C(10)-C(11)	2.1(2)
C(9)-C(10)-C(11)-C(12)	-1.8(2)
C(10)-C(11)-C(12)-C(13)	-1.2(2)
C(11)-C(12)-C(13)-C(8)	3.9(2)
C(11)-C(12)-C(13)-C(14)	-174.40(13)
C(9)-C(8)-C(13)-C(12)	-3.53(19)
C(7)-C(8)-C(13)-C(12)	177.90(12)
C(9)-C(8)-C(13)-C(14)	174.92(12)
C(7)-C(8)-C(13)-C(14)	-3.66(18)
N(1)-C(1)-C(14)-N(2)	0.24(14)
C(2)-C(1)-C(14)-N(2)	178.12(11)
N(1)-C(1)-C(14)-C(13)	-177.98(11)
C(2)-C(1)-C(14)-C(13)	-0.1(2)
C(12)-C(13)-C(14)-C(1)	-178.54(13)
C(8)-C(13)-C(14)-C(1)	3.11(19)
C(12)-C(13)-C(14)-N(2)	3.8(2)
C(8)-C(13)-C(14)-N(2)	-174.60(13)
N(1)-C(15)-C(16)-C(17)	97.27(18)
N(2)-C(15)-C(16)-C(17)	-86.86(17)
N(1)-C(15)-C(16)-C(25)	-81.47(18)
N(2)-C(15)-C(16)-C(25)	94.40(16)
C(25)-C(16)-C(17)-C(18)	1.2(2)
C(15)-C(16)-C(17)-C(18)	-177.51(15)
C(16)-C(17)-C(18)-C(19)	-1.6(3)
C(17)-C(18)-C(19)-C(20)	0.4(3)
C(18)-C(19)-C(20)-C(21)	-178.89(18)
C(18)-C(19)-C(20)-C(25)	1.1(3)
C(19)-C(20)-C(21)-C(22)	-179.33(18)
C(25)-C(20)-C(21)-C(22)	0.7(3)
C(20)-C(21)-C(22)-C(23)	0.3(3)
C(21)-C(22)-C(23)-C(24)	-0.7(3)
C(22)-C(23)-C(24)-C(25)	0.0(3)
C(23)-C(24)-C(25)-C(20)	1.0(2)
C(23)-C(24)-C(25)-C(16)	-178.90(14)
C(19)-C(20)-C(25)-C(24)	178.66(15)

C(21)-C(20)-C(25)-C(24)	-1.3(2)
C(19)-C(20)-C(25)-C(16)	-1.4(2)
C(21)-C(20)-C(25)-C(16)	178.58(14)
C(17)-C(16)-C(25)-C(24)	-179.80(14)
C(15)-C(16)-C(25)-C(24)	-1.1(2)
C(17)-C(16)-C(25)-C(20)	0.3(2)
C(15)-C(16)-C(25)-C(20)	179.02(12)
C(31)-C(26)-C(27)-C(28)	2.2(2)
N(2)-C(26)-C(27)-C(28)	-176.51(12)
C(26)-C(27)-C(28)-C(29)	-0.8(2)
C(27)-C(28)-C(29)-O(1)	177.63(14)
C(27)-C(28)-C(29)-C(30)	-1.2(2)
O(1)-C(29)-C(30)-C(31)	-177.10(14)
C(28)-C(29)-C(30)-C(31)	1.9(2)
C(29)-C(30)-C(31)-C(26)	-0.5(2)
C(27)-C(26)-C(31)-C(30)	-1.6(2)
N(2)-C(26)-C(31)-C(30)	177.13(13)
N(2)-C(15)-N(1)-C(1)	-0.98(15)
C(16)-C(15)-N(1)-C(1)	175.20(13)
C(14)-C(1)-N(1)-C(15)	0.43(15)
C(2)-C(1)-N(1)-C(15)	-177.31(13)
N(1)-C(15)-N(2)-C(14)	1.15(15)
C(16)-C(15)-N(2)-C(14)	-175.22(11)
N(1)-C(15)-N(2)-C(26)	176.90(11)
C(16)-C(15)-N(2)-C(26)	0.5(2)
C(1)-C(14)-N(2)-C(15)	-0.80(14)
C(13)-C(14)-N(2)-C(15)	177.21(13)
C(1)-C(14)-N(2)-C(26)	-176.39(12)
C(13)-C(14)-N(2)-C(26)	1.6(2)
C(27)-C(26)-N(2)-C(15)	-98.37(16)
C(31)-C(26)-N(2)-C(15)	82.92(17)
C(27)-C(26)-N(2)-C(14)	76.45(17)
C(31)-C(26)-N(2)-C(14)	-102.27(17)
C(28)-C(29)-O(1)-C(32)	-0.2(2)
C(30)-C(29)-O(1)-C(32)	178.73(15)

Symmetry transformations used to generate equivalent atoms: